# Uneven mitochondrial segregation during embryonic neurogenesis

**Benjamin Bunel [1,2], Rosette Goiame [1], Xavier Morin [3*], Evelyne Fischer [4*]**

1 : Institut de Biologie de l'Ecole Normale Supérieure (IBENS), CNRS, Inserm, Ecole Normale Supérieure, PSL Research University, 75005 Paris, France.

2 : Sorbonne Université, Collège Doctoral, 75005 Paris, France.

3 : Institut de Biologie de l'Ecole Normale Supérieure (IBENS), CNRS, Inserm, Ecole Normale Supérieure, PSL Research University, 75005 Paris, France. Electronic address: xavier.morin@ens.fr

4 : Institut de Biologie de l'Ecole Normale Supérieure (IBENS), CNRS, Inserm, Ecole Normale Supérieure, PSL Research University, 75005 Paris, France. Electronic address: evelyne.fischer@ens.fr

* : co-last authors ; co-corresponding authors

Keywords: neurogenesis, asymmetric cell division, mitochondria, cell fate determinant

**Abstract**

Asymmetric divisions of vertebrate neural progenitors are critical for generating neurons while preserving the stem cell pool, ensuring proper central nervous system development. It was previously shown that the remodeling of mitochondrial activity in daughter cells influences neural fates. In this study, we demonstrate that unequal mitotic distribution of mitochondria themselves plays a decisive role in triggering this differentiation process. Using live imaging to monitor mitochondrial segregation and track cell fates within embryonic neural tissue, we show that daughter cells inheriting fewer mitochondria consistently differentiate into neurons, whereas those receiving more mitochondria retain their progenitor status. Furthermore, experimental manipulation of mitochondrial inheritance during mitosis was sufficient to drive premature neuronal differentiation. Our findings establish a direct causal link between mitochondrial inheritance and the asymmetric fate of sister cells in vivo, highlighting a key mechanism in neural development.

## Main text

Asymmetric divisions are a fundamental characteristic of stem cells, relying on the unequal inheritance of fate determinants that drive differentiation of one progeny while simultaneously maintaining stemness in the other daughter. During vertebrate central nervous system development, the process of neuronal differentiation entails remodeling of mitochondrial functions and metabolism that control downstream gene regulatory pathways (Iwata et al., 2020; Khacho et al., 2016). Notably, fate decisions in the progeny of cortical progenitors depend on modifications in the balance between mitochondrial fusion and fission taking place within a brief time window following cell division (Iwata et al., 2020). This raises the question of what triggers these mitochondrial changes: are they instructed after mitosis downstream of non-mitochondrial fate determinants (Tozer et al, 2017, Coumailleau et al, 2009, Richard et al, 2024) or are they independently encoded in an asymmetric mitochondrial behavior within the dividing mother cell?

## Uneven mitochondrial segregation during neurogenesis

We used live imaging in the embryonic chick neural tube to study mitochondrial segregation during neural progenitor divisions. Constructs expressing fluorescent proteins fused to the mitochondrial targeting sequence of Cox8 were electroporated in ovo (Figure 1A) and mitochondrial inheritance was monitored ex ovo in "en-face" live imaging of the apical surface of the spinal neuroepithelium (Figure 1B), where divisions occur. Using 4D confocal microscopy, we monitored mitochondria and cell contours through the whole mitotic sequence at 3min time intervals (Figure 1B, Supplementary Figure 1A). Mitochondrial volumes were reconstructed and measured in each of the two sister cells immediately after cytokinesis, and mitochondrial inheritance was assessed using a metric termed $R_{mito}$, which represents the ratio of the smaller to the larger of these two values (Supplementary Figure 1B). As an example, a $R_{mito}$ value of 1 indicates that each daughter cell inherits 50% of the mother's mitochondrial pool, whereas a Rmito value of 0.5 indicates that one cell inherits twice as many mitochondria as its sister cell. (Figure 1C, Supplementary Figure 1A). We first monitored mitochondrial inheritance at embryonic day 3 (E3, HH17-18), and found that $R_{mito}$ distributed across a broad range of values between 1 and 0.5 (Figure 1D). At that stage, three modes of progenitor divisions exist in the spinal cord: symmetric proliferative divisions (producing two progenitors:

PP), asymmetric neurogenic divisions (producing a progenitor and a neuron: PN), and rare symmetric terminal neurogenic divisions (producing two neurons: NN) (Saade et al, 2013; Le Dreau et al., 2014).

We wondered whether the broad distribution observed at E3 might be linked to the coexistence of the three modes of division. To test his hypothesis, we monitored mitochondrial inheritance at E2, when the symmetric PP mode of division strongly predominates. We found that mitochondria were mostly distributed evenly between sister cells, contrasting with the high frequency of uneven inheritance observed at E3 (Figure 1D). Conversely, we monitored mitochondrial inheritance in a population enriched for progenitors undergoing asymmetric PN divisions, identified at E3 thanks to the targeted insertion of a Cre recombinase at the Tis21 locus (Hämmerle et al., 2002; Iacopetti et al., 1999; Saade et al., 2013, Petit-Vargas et al., 2024) (Figure 1D and Materials and Methods). In this subpopulation, the distribution of $R_{mito}$ values shifted significantly towards more unequal values compared to the whole progenitor population at E3.

Is unequal mitochondrial segregation a reflection of a global difference in size between sister cells? To answer this question, we monitored both mitochondrial and cellular volumes upon cytokinesis in pairs of Tis21-Cre sisters. In this dataset, which displays the highest proportion of unequal mitochondrial inheritance, the cellular volume was nearly identical between sisters, indicating that these two parameters are uncoupled (Supplementary Figure 2). These findings confirm that unequal mitochondrial segregation constitutes an independent factor.

Thus, we observe an increase in uneven mitochondrial inheritance between pairs of sister cells that mirrors the expected rise in the proportion of asymmetric modes of division among the E2, E3 and E3-Tis21 populations (Figure 1D) (Saade et al., 2013, le Dreau 2014, Petit-Vargas et al., 2024).

**Unequal mitochondrial segregation is a hallmark of asymmetric divisions**

Next we asked whether challenging a progenitor's mode of division would impact the distribution of mitochondria. Modulating the expression of cell cycle regulators in progenitors has been used to artificially accelerate or delay the onset of neurogenic modes of divisions (Bonnet et al., 2018; Lange et al., 2009; Pilaz et al., 2009). We first experimentally forced premature neurogenic divisions at early stages by overexpressing the CDC25b phosphatase, a G2/M regulator (Bonnet et al., 2018). This led to a significant shift towards unequal mitochondrial inheritance: the distribution of $R_{mito}$ in CDC25b overexpressing cells at E2.5 was

significantly different from the control (Figure 2A), and closely resembled what is normally observed at later stages (see Figure 1D). This higher proportion of unequal mitochondrial inheritance was accompanied by an increased production of neurons 12 hours later (Supplementary Figure 3), consistent with a premature onset of asymmetric modes of division at that stage. Conversely, we sought to promote symmetric proliferative divisions by knocking-down the G1 regulator CDKN1C/p57$^{kip2}$, which delays neurogenesis by favoring this mode of division (Mida et al., 2024). Remarkably, this significantly reduced the proportion of unequal mitochondrial inheritance at E3 (Figure 2B), and led to a distribution of $R_{mito}$ that closely matched what is normally observed at E2 (Figure 1D).

We next investigated whether uneven partitioning of mitochondria is directly associated with an asymmetric cell fate. We monitored mitochondrial inheritance in individual progenitors as described above and tracked fate acquisition in their daughter cells through additional imaging for 20 to 30 hours. A new division event identifies a daughter cell as a progenitor (P), whereas delamination from the apical surface characterizes a differentiating neuron (N) (Tozer et al., 2017), and see Materials and Methods; Figure 2C-D and Supplementary Figure 4).

Our results from 58 pairs of cells show that the distribution of $R_{mito}$ differs between symmetrically and asymmetrically dividing progenitors (Figure 2E). In the symmetrically dividing population (PP and NN divisions, n=24 cells), the values of $R_{mito}$ were homogenously distributed in the 0.85 to 1 range, with the exception of two outliers. We therefore propose a threshold at 0.85 that will be used henceforth to define equal versus unequal mitochondrial inheritance. In stark contrast to symmetric divisions, the values of $R_{mito}$ in asymmetric divisions were distributed between 0.55 and 1, with the majority of PN daughters (n=23/34) receiving unequal mitochondrial pools ($R_{mito} < 0.85$) (Figure 2E). This live analysis, which directly links mitotic events in the progenitor to post mitotic cellular identity in its progeny, shows that an unequal mitochondrial inheritance is a strong - albeit not absolute - predictor of an asymmetric fate decision. One additional feature of the individual tracking of pairs of cells is that it enables to discern which daughter cell, of the neuron or the progenitor, receives the largest or smallest mitochondrial pool. We observed a compelling near-exclusive relationship between mitochondrial pool size and fate: in 21 out of the 23 PN divisions showing unequal mitochondrial inheritance, the sister cell receiving fewer mitochondria differentiated into a neuron (Figure 2E and 2F).

Our analysis of pairs of sister cells, and in particular the striking ‘directionality’ of mitochondrial distribution that we observed during asymmetric neurogenic division, further

supports the idea that the unequal partitioning of mitochondria during mitosis initiates different mitochondria-regulated programs between progenitors and neurons during embryonic neurogenesis.

## Uneven mitochondrial segregation drives differential fate choices

We then investigated whether the relationship between unequal mitochondrial inheritance and differential fate acquisition is causal. An effective approach involves directly manipulating mitochondrial distribution to induce unequal inheritance in proliferative progenitors that normally distribute them equally, and subsequently assessing the impact on the identity of their progeny.

### *Forcing unequal mitochondrial segregation via artificial attachment to the microtubular network*

Previous studies have shown that mitochondrial partitioning during mitosis is essentially symmetric in cultured cell lines, driven by mechanisms including the actin and microtubule networks and their motor proteins (Chung et al., 2016; Moore et al., 2021; Rohn et al., 2014). Strikingly, artificially tethering mitochondria to a kinesin to force their attachment to the microtubule network during mitosis disrupts the control of their symmetric distribution to daughter cells (Chung et al., 2016). We developed a time-controlled adaptation of this strategy to restrict the forced attachment of mitochondria to the microtubule network to a time window around progenitor mitosis (Figure 3A), and avoid long-lasting effects on mitochondrial motility in their progeny. We used the CatchFire (chemically assisted tethering of chimera by fluorogenic-induced recognition) method, to induce the rapid and reversible association of mitochondria with a plus-end directed kinesin motor upon application and removal of a specific ligand (Bottone et al., 2023).

We electroporated vectors expressing the mitochondrial and kinesin moieties of the CatchFire dimer (thereafter MitoFireMate and KifFireTag, respectively, Figure 3A) together with fluorescent mitochondrial and membrane reporters, and assessed mitochondrial behavior following administration of the ligand in en-face live preparations. Within 15 minutes of ligand exposure, mitochondria located more basally than in controls and appeared more compacted from metaphase until cytokinesis (Supplementary Figure 5 and Supplementary Figure 6A). Most importantly, this led to unequal mitochondrial segregation, including extreme $R_{mito}$ values lower than 0.5 (Supplementary Figure 6B), demonstrating that the CatchFire approach

reproduces in vivo what has been observed upon artificial tethering of mitochondria to a kinesin in vitro (Chung et al., 2016). We then calibrated the ligand administration regime to obtain $R_{mito}$ values contained within the physiological range observed in asymmetrically dividing progenitors, and to restrict this effect to the approximate duration of mitosis (see Materials and Methods for details). With this optimized protocol, we monitored mitotic events at E2, when a majority of progenitors undergo PP divisions and mitochondrial inheritance is mostly equal (Figure 1D). We observed a significant shift towards unequal inheritance in ligand-treated cells, whereas the great majority of cells dividing before and after ligand exposure displayed the characteristic equal mitochondrial segregation normally observed at that stage (Figure 3B and Supplementary Figure 6C; see also Figure 1D). Of note, cells that retained a $R_{mito}$ value higher than 0.85 during ligand exposure did not display any mitochondrial compaction (Supplementary Figure 6D-F), suggesting that these cells did not receive the two components of the CatchFire system, as can happen when multiple vectors are co-electroporated.

The range of experimentally-induced $R_{mito}$ values obtained at E2 with this molecular toolkit is comparable to what is observed at E3 and E4 (Figure 1D) and should not compromise daughter cell survival. Hence, the powerful CatchFire approach that we have developed offers a unique opportunity to unravel the functional link between mitochondrial distribution and cell fate decisions.

***Forcing unequal mitochondrial segregation is sufficient to induce asymmetric fate choices***

In the next series of experiments, we combined CatchFire manipulation of mitochondrial distribution with daughter cell fate tracking. We first monitored mitochondrial distribution in progenitors undergoing mitosis during the 1hr period of CatchFire ligand activity. In addition to these early-stage analyses, we used two alternative sets of prolonged live imaging to establish cell fates. In one of them, we tracked daughter cells for 24 to 30 hours, allowing identity to be assigned from a new round of mitosis or an apical detachment, as described above. In the other set of tracking experiments, we imaged daughter cells up to 2.5 hours after mitosis, then fixed the samples and used immunofluorescence to assign an identity. We took advantage of the differential expression of the hyperphosphorylated form of the Retinoblastoma protein (pRb), which is detected in all cycling progenitors (see methods), whereas future neurons remain negative for this marker (Mida et al, 2024). Daughter cells positive or negative for pRb at the end of the 2.5 hours tracking period could therefore be identified as a progenitor (P) or a neuron (N), respectively (Figure 3D and Supplementary Figure 7).

In these experiments, mitochondrial segregation was again unequal in a majority (20 out of 36) of CatchFire ligand-treated pairs of cells, contrasting with an equal distribution in most pairs of untreated control cells (33 out of 40) (Figure 3E, Supplementary Figure 8A). Remarkably, this was accompanied by a dramatic increase in the proportion of asymmetric PN divisions, with more than half of the CatchFire ligand-treated pairs (19/36) showing one sister cell committed to differentiation, compared to only 20% (8/40) in the control condition (Figure 3F, Supplementary Figure 8B).

The premature shift toward a neuronal fate in one of the daughter cells was specific of pairs of sister cells with experimentally induced unequal mitochondrial inheritance (Figure 3G, Supplementary Figure 8C). This was even more compelling when focusing on the 15 pairs with increased mitochondrial compaction (squares in Figure 3G): CatchFire induced a different sister fate (PN) in 12 of these pairs, and the only pair exhibiting equal mitochondrial inheritance maintained a symmetric PP fate (Figure 3G).

Additionally, the relationship between mitochondrial volume inheritance and fate determination was conserved: the smaller mitochondrial pool was inherited by the future neuron in 10 of these 12 PN pairs (Figure 3G), consistent with our observations in asymmetrically dividing progenitors at E3 (Figure 2E).

Overall, these results show that an experimentally induced mitochondrial imbalance during division is sufficient to induce a neurogenic fate in the daughter cell that inherits fewer mitochondria.

Our observations in neural progenitors reveal a causal relationship between unequal mitochondrial volume apportioning and asymmetric fate acquisition. This finding diverges from earlier studies in adult stem cell systems, primarily in vitro, which correlated the inheritance of qualitatively distinct mitochondrial pools with distinct daughter cell proliferative capacities (Döhla et al., 2022; Adams et al., 2016; Borsa et al., 2024; Hinge et al., 2020; Katajisto et al., 2015). This discrepancy raises an intriguing question: could the observed quantitative difference be a distinctive feature of a developmental context, distinct from adult stem cells, which are likely influenced by the constraints of protection against aging processes and the accumulation of damaged proteins and organelles? Consistent with this idea, our data in the embryonic neural tube provide evidence that engineering an unequal mitochondrial volume distribution is sufficient to induce asymmetric fates at a stage when this typically does

not occur, whereas there was no evidence of quantitative differences in mitochondrial volumes between sister cells in adult mammary gland stem cells (Katajisto et al., 2015).

We show that inheritance of a smaller mitochondrial volume is associated with and sufficient to induce neuronal differentiation. How does it cause a fate switch? One possibility is that a smaller mitochondrial pool causes an energetic or metabolic deficiency after mitosis. This may redirect the mitochondrial pool towards OXPHOS metabolism, resulting in a rise in neural differentiation pathways (Iwata et al., 2020; Khacho et al., 2016) and concomitant repression of progenitor pathways (Bonnefont et al., 2019; Tiberi et al., 2012). In parallel, this initial signal may trigger the progressive increase of mitochondrial mass that is observed later during differentiation (Iwata et al., 2023). This proposed mechanism, whereby a reduced mitochondrial volume at a critical stage in the cell cycle primes cells for a differentiation-specific metabolic shift, may represent an underexplored pathway that links mitochondria to cellular fate decisions in a developmentally regulated, stage-specific manner.

Other determinants have been involved in asymmetric fate decisions in neural progenitors (Coumailleau et al., 2009; Richard et al., 2024; Tozer et al., 2017). Whether and how mitochondria interact with the pathways downstream of these determinants will represent an exciting challenge for future research.

## References


Benaissa, H., Ounoughi, K., Aujard, I., Fischer, E., Goïame, R., Nguyen, J., Tebo, A.G., Li, C., Le Saux, T., Bertolin, G., Tramier, M., Danglot, L., Pietrancosta, N., Morin, X., Jullien, L., Gautier, A., 2021. Engineering of a fluorescent chemogenetic reporter with tunable color for advanced live-cell imaging. Nat Commun 12, 6989. https://doi.org/10.1038/s41467-021-27334-0

Bonnefont, J., Tiberi, L., Van Den Ameele, J., Potier, D., Gaber, Z.B., Lin, X., Bilheu, A., Herpoel, A., Velez Bravo, F.D., Guillemot, F., Aerts, S., Vanderhaeghen, P., 2019. Cortical Neurogenesis Requires Bcl6-Mediated Transcriptional Repression of Multiple Self-Renewal-Promoting Extrinsic Pathways. Neuron 103, 1096-1108.e4. https://doi.org/10.1016/j.neuron.2019.06.027

Bonnet, F., Molina, A., Roussat, M., Azais, M., Bel-Vialar, S., Gautrais, J., Pituello, F., Agius, E., 2018. Neurogenic decisions require a cell cycle independent function of the CDC25B phosphatase. Elife 3;7:e32937. https://doi.org/10.7554/eLife.32937.

Bottone, S., Cakil, Z.V., Joliot, O., Boncompain, G., Perez, F., Gautier, A., 2023. A fluorogenic chemically induced dimerization technology for controlling, imaging and sensing protein proximity (preprint). Cell Biology. https://doi.org/10.1101/2023.01.04.522617

Chung, J.Y.-M., Steen, J.A., Schwarz, T.L., 2016. Phosphorylation-Induced Motor Shedding Is Required at Mitosis for Proper Distribution and Passive Inheritance of Mitochondria. Cell Reports 16, 2142–2155. https://doi.org/10.1016/j.celrep.2016.07.055

Cong, L., Ran, F.A., Cox, D., Lin, S., Barretto, R., Habib, N., Hsu, P.D., Wu, X., Jiang, W., Marraffini, L.A., Zhang, F., 2013. Multiplex genome engineering using CRISPR/Cas systems. Science 339, 819–823. https://doi.org/10.1126/science.1231143

Edelstein, A., Amodaj, N., Hoover, K., Vale, R., Stuurman, N., 2010a. Computer control of microscopes using µManager. Curr Protoc Mol Biol Chapter 14, Unit14.20. https://doi.org/10.1002/0471142727.mb1420s92

Edelstein, A., Amodaj, N., Hoover, K., Vale, R., Stuurman, N., 2010b. Computer control of microscopes using µManager. Curr Protoc Mol Biol Chapter 14, Unit14.20. https://doi.org/10.1002/0471142727.mb1420s92

Iwata, R., Casimir, P., Erkol, E., Boubakar, L., Planque, M., Gallego López, I.M., Ditkowska, M., Gaspariunaite, V., Beckers, S., Remans, D., Vints, K., Vandekeere, A., Poovathingal, S., Bird, M., Vlaeminck, I., Creemers, E., Wierda, K., Corthout, N., Vermeersch, P., Carpentier, S., Davie, K., Mazzone, M., Gounko, N.V., Aerts, S., Ghesquière, B., Fendt, S.-M., Vanderhaeghen, P., 2023. Mitochondria metabolism sets the species-specific tempo of neuronal development. Science 379, eabn4705. https://doi.org/10.1126/science.abn4705

Iwata, R., Casimir, P., Vanderhaeghen, P., 2020. Mitochondrial dynamics in postmitotic cells regulate neurogenesis. Science 369, 858–862. https://doi.org/10.1126/science.aba9760

Khacho, M., Clark, A., Svoboda, D.S., Azzi, J., MacLaurin, J.G., Meghaizel, C., Sesaki, H., Lagace, D.C., Germain, M., Harper, M.-E., Park, D.S., Slack, R.S., 2016. Mitochondrial Dynamics Impacts Stem Cell Identity and Fate Decisions by Regulating a Nuclear

Transcriptional Program. Cell Stem Cell 19, 232–247. https://doi.org/10.1016/j.stem.2016.04.015

Lange, C., Huttner, W.B., Calegari, F., 2009. Cdk4/cyclinD1 overexpression in neural stem cells shortens G1, delays neurogenesis, and promotes the generation and expansion of basal progenitors. Cell Stem Cell 5, 320–331. https://doi.org/10.1016/j.stem.2009.05.026

Mida, B., Lehman, N., Coulpier, F., Bouhali, K., Goiame, R., Thomas-Chollier, M., Fischer, E., Morin, X., 2024. A low CDKN1c/p57$^{kip2}$ expression in spinal progenitors drives the transition from proliferative to neurogenic modes of division. https://doi.org/10.1101/2024.10.10.617342

Moore, A.S., Coscia, S.M., Simpson, C.L., Ortega, F.E., Wait, E.C., Heddleston, J.M., Nirschl, J.J., Obara, C.J., Guedes-Dias, P., Boecker, C.A., Chew, T.-L., Theriot, J.A., Lippincott-Schwartz, J., Holzbaur, E.L.F., 2021. Actin cables and comet tails organize mitochondrial networks in mitosis. Nature 591, 659–664. https://doi.org/10.1038/s41586-021-03309-5

Morin, X., Jaouen, F., Durbec, P., 2007. Control of planar divisions by the G-protein regulator LGN maintains progenitors in the chick neuroepithelium. Nat Neurosci 10, 1440–1448. https://doi.org/10.1038/nn1984

Petit-Vargas, A.P., Mida, B., Goïame, R., Alegria-Prevot, O., Djelic, B., Fischer, E., Tozer, S., Gros, J., Manceau, M., Morin, X., 2024. CRISPR/Cas9-based somatic knock-in of reporters in the avian embryo in ovo. https://doi.org/10.1101/2024.10.10.617291

Pilaz, L.-J., Patti, D., Marcy, G., Ollier, E., Pfister, S., Douglas, R.J., Betizeau, M., Gautier, E., Cortay, V., Doerflinger, N., Kennedy, H., Dehay, C., 2009. Forced G1-phase reduction alters mode of division, neuron number, and laminar phenotype in the cerebral cortex. Proc. Natl. Acad. Sci. U.S.A. 106, 21924–21929. https://doi.org/10.1073/pnas.0909894106

Rohn, J.L., Patel, J.V., Neumann, B., Bulkescher, J., Mchedlishvili, N., McMullan, R.C., Quintero, O.A., Ellenberg, J., Baum, B., 2014. Myo19 ensures symmetric partitioning of mitochondria and coupling of mitochondrial segregation to cell division. Curr Biol 24, 2598–2605. https://doi.org/10.1016/j.cub.2014.09.045

Schneider, C.A., Rasband, W.S., Eliceiri, K.W., 2012. NIH Image to ImageJ: 25 years of image analysis. Nat Methods 9, 671–675. https://doi.org/10.1038/nmeth.2089

Tiberi, L., Van Den Ameele, J., Dimidschstein, J., Piccirilli, J., Gall, D., Herpoel, A., Bilheu, A., Bonnefont, J., Iacovino, M., Kyba, M., Bouschet, T., Vanderhaeghen, P., 2012. BCL6 controls neurogenesis through Sirt1-dependent epigenetic repression of selective Notch targets. Nat Neurosci 15, 1627–1635. https://doi.org/10.1038/nn.3264

Tozer, S., Baek, C., Fischer, E., Goiame, R., Morin, X., 2017. Differential Routing of Mindbomb1 via Centriolar Satellites Regulates Asymmetric Divisions of Neural Progenitors. Neuron 93, 542-551.e4. https://doi.org/10.1016/j.neuron.2016.12.042

**Acknowledgements**

We thank Samuel Tozer for insightful discussions on the project, and our colleagues Jean-François Brunet, Sonia Garel, Alice Meunier, Jonathan Weitzman, Marco Pontoglio and Samuel Tozer for their comments on the manuscript. We thank Fabienne Pituello for the kind gift of CDC25B plasmids, and Octave Joliot, Franck Perez and Arnaud Gautier for generously sharing unpublished components of the CatchFire system. We thank the IBENS imaging platform for access to the IMARIS analysis station. **Funding**: work in the Morin lab is supported by grants from the Agence Nationale de la Recherche (SYMASYM ANR-18-CE16-0021-01), the Fondation pour la Recherche Médicale (FRM EQU202003010547) and the Labex MEMOLIFE. This work has received support under the program « Investissements d'Avenir » launched by the French Government and implemented by the ANR, with the reference ANR-10-LABX-54 MEMO LIFE. **Authors contributions:** Conceptualization: E.F.; Formal analysis: B.B., E.F.; Funding acquisition: X.M.; Investigation: B.B., R.G., X.M., E.F.; Methodology: B.B., X.M., E.F.; Project administration: E.F.; Supervision: E.F.; Validation: E.F.; Visualization: B.B., X.M.; Writing – original draft: E.F.; Writing – review & editing: X.M. and E.F.

**Competing interests**: the authors declare no competing interests

**Data and materials availability:** All data are available in the manuscript or the supplementary materials. Plasmids used in this study and the full sequences are available upon request to X.M.

**List of Supplementary Materials**

Materials and Methods

Figs. S1 to S8

Table S1

## Materials and methods

### Embryos

JA57 chicken fertilized eggs were provided by EARL Morizeau (8 rue du Moulin, 28190 Dangers, France). They were incubated at 38 °C in a Sanyo MIR-253 incubator for the appropriate time.

### In ovo electroporation

In ovo electroporations in the chick neural tube were performed at embryonic day 1.5 (E1.5, HH stage 10) or E2 (E2, HH stage 14). The DNA solution, containing the vital dye FastGreen for visualization, was injected directly into the lumen of the neural tube via glass capillaries. Five 50ms pulses of 20V (at E1.5) or 25V (at E2) separated by 100 ms intervals were applied using a square-wave electroporator (Nepa Gene, CUY21SC) and a pair of 5 mm gold-plated electrodes (BTW Genetrode model 512) separated by a 4 mm interval. The egg was then sealed with parafilm and returned to the incubator.

**Plasmids**

A list of plasmids used in this study is presented in Table 1

Mitochondrial reporters: the Mitobow construct (X503) has been described in Loulier et al, 2014.

pCX-lox-H2B-EBFP2-lox-mitoGFP (X1017, lox-mito-GFP in Figures) was created as follows: a pCX-lox-H2B-EBFP2-lox-mitoCerulean vector (X992) was first generated by deletion of a SacI-PmlI fragment from Mitobow construct. A lox-H2B-EBFP2-polyA-lox-mito PCR fragment was then amplified from X992 with the following oligonucleotides (CX-fw 5'-GTCTCATCATTTTGGCAAAGAATTCTAGCT-3' and GFP-Eco-mito-rev 5'-CCTTGCTCACCATGGTGGCGAATTCGGAGGTGGCGACGG-3') and Gibson cloned into NheI/AgeI digested X-013 (pCX-GFP, Morin et al, 2007).

pCX-mito-Cherry (X1202, mito-Cherry in Figures) was created as follows: a pCX-lox-mito-Cherry-lox-mito-Cerulean vector (X993) was first generated by deletion of a SmaI-PacI fragment from Mitobow construct. A lox-mitoCherry-polyA-lox-mito PCR fragment was then amplified from X993 with CX-fw and GFP-Eco-mito-rev oligonucleotides and Gibson cloned into NheI/AgeI digested X-013 (pCX-GFP, Morin et al, 2007) to construct X-1118. pCX-mito-Cherry (X1202) was obtained by removing the BsrGI (stop-lox-mito-GFP) fragment from X-1118.

CatchFire plasmids: pK-Tom20-FireMate and pK-Kif17a-FireTag (unpublished vectors related to Bottone et al., 2023, generously provided by Frank Perez and Octave Joliot) were modified for optimized expression in the chick neural tube by replacing the CMV promoter with a CAGGS (CX) promoter. To generate pCX-Tom20-FireMate (MitoFireMate in Figures), the CMV promoter in pK-Tom20-FireMate was replaced by the Nde1/Nhe1 CAGGS promoter fragment from pCX-MCS2 (Morin et al., 2007). To generate pCX-Kif17a-FireTag (KifFireTag in Figures), the CMV promoter in pK-Kif17a-FireTag was replaced by a Nde1/Mfe1 fragment from pCX-H2B-miRFP670.

Membrane contours: pCX-mb-GFP-ires-H2B-GFP and pCX-mb-iRFP670.

Apical staining: pCX-ZO1-miRFP670.

PMP-CDC25b, PMP-lacZ were kind gifts from Fabienne Pituello's Lab. The shCDKN1c vector (X1101, Mida et al, in preparation) contains a chick CDKN1c miRNA under the control of chick U6 promoter, H2BGFP under control of CAGGS promoter.

Somatic knock-in of the Cre recombinase at the Tis21 locus:

Somatic knock-in of the Cre recombinase coding sequence at the C-terminus of the Tis21 locus was achieved via CRISPR-Cas9-based Homology-Directed Recombination (HDR), through co-electroporation of a donor vector (Tis21-P2A-Cre, X907) and a CRISPR/Cas9 vector expressing the Cas9 recombinase and a gRNA targeting the C-terminus of the Tis21 locus (pCX-SpCas9-cTis21-gRNA2, X854). The Tis21 gRNA targets the cttggcagtgtaaggacaag sequence on the antisense strand and cuts 11 bases downstream of the Tis21 stop codon. It was cloned in the BpiI-linearized X330 vector as described (Cong et al., 2013) using a duplex of oligonucleotides Tis21-gRNA2-fw (5'-CACCGCTTGGCAGTGTAAGGACAAG-3') and Tis21-gRNA2-rev (5'-AAACCTTGTCCTTACACTGCCAAGC-3'). The Tis21-P2A-Cre donor vector consists of a P2A-Cre cassette flanked with long left (1010bp) and right (971bp) arms of homology to the C-terminal region of chick Tis21 (bGalGal1.mat.broiler.GRCg7b genome assembly). The P2A pseudo-cleavage sequence ensures that the Tis21 protein and Cre recombinase are produced as two independent proteins. In order to prevent targeting of the knock-in plasmid and re-targeting of the locus after insertion of the knock-in cassette by the gRNA, the gRNA target sequence was destroyed in the right arm of homology via the introduction of 7 bases changes. Full detail of the construction of this vector and of its validation as a bona fide Tis21 targeting vector are described in Petit-Vargas et al (DOI à venir).

***Plasmid concentrations for mitochondrial distribution at different stages of neurogenesis and functional challenges***

For E2 experiments, pCX-mb-GFP-ires-H2B-GFP (0.5µg/µl) and pCX-mito-Cherry (0.3µg/µl) were electroporated at E1.5.

For E3 and E4 experiments, either pCX-mito-CFP (0.5µg/µl) or a mix of Mitobow (0.5µg/µl) and pCX-Cre (0.1µg/µl) were electroporated with pCX-mb-iRFP670 (0.3µg/µl) at E2.

For E5 experiments, pCX-mito-Cherry (0.5µg/µl) and pCX-mb-iRFP670 (0.5µg/µl) were electroporated at E2.

For measurements in Tis21 positive progenitors at E3, Tis21-P2A-Cre donor and pCX-SpCas9-cTis21-gRNA2 vectors were each used at 0.8 µg/µl in the electroporation mix. The pCX-lox-

H2B-EBFP2-lox-mito-GFP reporter plasmid (0.3µg/µl) and pCX-mb-iRFP670 (0.5µg/µl) were added to the electroporation mix.

For experiments forcing premature neurogenic divisions at E2.5, pCX-mb-GFP-ires-H2B-GFP (0.5µg/µl), pCX-mito-Cherry (0.3µg/µl) and either PMP-CDC25b (1µg/µl) or the control vector PMP-lacZ (1µg/µl), were electroporated at 1.5.

For experiments forcing symmetric proliferative divisions at E3, pCX-mb-iRFP670 (0.5µg/µl), pCX-mito-Cherry (0.3µg/µl) and sh-CDKN1c (1µg/µl) were electroporated at E2.

***Plasmid concentrations for neurogenesis rate measurements***

E1.5 embryos were electroporated with pCX-H2B-GFP (0.3µg/µl) and either PMP-CDC25b (1µg/µl) or PMP-lacZ (1µg/µl) for controls and they were harvested 30 hours after electroporation.

***Plasmid concentration for fate tracking in Tis21+ progenitors***

E2 embryos were electroporated with Cytobow (0.3µg/µl), pCX-lox-H2B-EBFP2-lox-mito-GFP (0.3µg/µl), pCX-ZO1-miRFP670 (0.3_µg/µl), Tis21-P2A-Cre (0.8µg/µl) and pCX-SpCas9-cTis21-gRNA2 (0.8µg/µl).

***Plasmid concentration for Catchfire experiments***

E1.5 embryos were electroporated with pCX-Tom20-FireMate (0.3µg/µl), pCX-Kif17-FireTag (0.3µg/µl), pCX-mb-GFP-ires-H2B-GFP (0.4µg/µl), pCX-mito-Cherry (0.4µg/µl) and pCX-ZO1-miRFP670 (0.4µg/µl).

**Imaging**

All the images in this study were obtained on an inverted microscope (Nikon Ti Eclipse) equipped with a spinning disk confocal head (Yokogawa CSUW1) with Borealis system (Andor) and a sCMOS Camera (Orca Flash4LT, Hamamatsu) and the following Nikon objectives: 10x (CFI Plan APO λ, 0.45), 40x (CFI Plan APO λ, 0.95) or 100x (CFI APO VC, NA 1.4, oil immersion). The setup is driven by MicroManager software (Edelstein et al., 2010a) and equipped with a heating enclosure (DigitalPixel, UK) set to 37.5°C for live imaging experiments.

**En-face culture**

En-face culture of the embryonic neuroepithelium was performed at different stages (E2.25, E2.5, E3, E4 and E5). After extraction from the egg and removal of extraembryonic membranes in 1xPBS (thereafter PBS), embryos were transferred to 37 °C F12 medium and pinned down

with dissection needles at the level of the hindbrain in a 35 mm Sylgard dissection dish. A dissection needle was used to slit the roof plate and separate the neural tube from the somites from hindbrain to caudal end on both sides of the embryo. The neural tube and notochord were then transferred in a drop of F12 medium to a glass-bottom culture dish (MatTek, P35G-0-14-C) and medium was replaced with 1ml of 1% low melting point agarose/F12 medium (maintained at 38°C). Excess medium was removed so that the neural tube would flatten with its apical surface facing the bottom of the dish, in an inverted open book conformation. After 30 seconds of polymerization on ice, an extra layer of agarose medium (200 µl) was added to cover the whole tissue and left to harden. 2ml of 38 °C culture medium was added (F12/1mM Sodium pyruvate) and the culture dish was transferred to the 38 °C chamber of a spinning disk confocal microscope.

***Live monitoring of mitochondria during cell divisions:***

Several full-frame fields of view (136*136µm) were selected on the flat mounted neural tube, and ~25µm deep z-stacks were acquired with a 0.3µm z-step size at 3 minutes intervals during 1 to 2 hours. Images were saved as separated images and imported in Fiji. Pairs of daughter cells at the first timepoint after division presenting both membrane or cytoplasmic reporter signal and mitochondrial signal were identified and selected to be cropped on their entire height. Selected crops were saved as image stack files for 3D reconstruction (see below).

***Daughter fate tracking experiments:***

For fate tracking experiments, an initial acquisition of images was performed using the parameters described above for mitochondrial monitoring for a duration of 1 to 2 hours, before switching to new acquisition parameters as detailed below.

Of note, mitochondrial ratio and daughter fates were determined independently in a blind manner within the whole set of pairs. Mode of division and mitochondrial inheritance were matched retrospectively.

For long term live tracking, the acquisition parameters were then modified as follows: ~25µm deep z-stacks centered around the apical surface were acquired with a 1µm z-step at 15 minutes intervals for 24 to 30 hours. To reduce potential phototoxicity, the mitochondrial channel was omitted during this sequence as it is not required for tracking. Using the apical surface marker (ZO1-miRFP670), we were then able to track daughter cells and assign their identity from their behavior: progressive apical constriction (over at least three consecutive time points) followed by apical detachment for a future neuron, versus apical surface division for a progenitor. The

purpose of keeping a large z-depth centered on the apical surface was to accommodate for potential z-drifting of the embryo relative to the coverslip during the long acquisition.

For tracking experiments combining short-term live tracking and immunostaining, we used the following protocol: we increased the depth of imaging to 50µm, and acquired 1µm-spaced z-stacks every 10 or 15 minutes for 2h30. We then switched to the 10x objective and acquired an extended field of view to acquire spatial landmarks in order to facilitate the repositioning of the culture dish with the same orientation after immunostaining. The culture dish was then removed from the microscope stage and immediately processed for fixation and immunostaining. The whole staining procedure was performed at 4°C, and we only subjected the samples to very gentle agitation to ensure that the neural tubes remained embedded in the 1% LMP agarose layer. The culture medium was removed, and the samples were quickly washed once in PBS before fixation for 90' in ice-cold 4% paraformaldehyde (PFA) in PBS followed by 3 washes of 15 minutes in PBS. The neural tube was incubated for 48h with the anti-pRb and anti-GFP primary antibodies in the blocking solution (PBS/0,3% Triton/10%Fetal Calf Serum (FCS)). The samples were then washed 3 times for 15 minutes in PBS and incubated for 48 hours in the dark with the secondary Cy5 anti-rabbit antibody (1/500) and DAPI (1/1000) in PBS/0,3% Triton. The samples were then washed 3 times for 15 minutes in PBS. 1 ml of PBS was added to the culture dish, which was subsequently transferred to the microscope. We first used the 10x objective to reposition the dish in the same orientation and recover each original field thanks to the 10x images acquired at the end of the 2h30 movie. We then switched to the 100x objective, and used the last images of the 100x live sequence to precisely recover the corresponding fields and acquire matching 4 channels z-stacks in the fixed and stained neural tube (405nm/DAPI; 490nm/mb-GFP and H2B-GFP; 561nm/mito-Cherry; 641nm/Cy5-pRb).

We then used the H2B-GFP signal in the live sequence to track daughter cells as their nucleus starts to move basally after mitosis. Briefly, for each field of view, we imported the stack files of the 1h and 2h30 live sequences in Fiji. We identified divisions of electroporated progenitors occurring during the 1h movie and we followed the nucleus of the daughters during the 2h30 movie. For each pair in which we were still able to visualize the nucleus in each sister cell at the last time point, we proceeded to analyze the corresponding 100x z-stack from the fixed sample and recovered these sister cells on the basis of their H2B-GFP signal. We then determined the identity of the two daughter cells on the basis of the pRb immunostaining in the far-red channel (pRb (+) = progenitor; pRb (-) = neuron).

The 2.5-hour time window was established beforehand in E2 embryos as follows: we determined the time point after mitosis at which pRb becomes a reliable progenitor marker by monitoring the time window after which all progenitors in a synchronized cohort of cells undergoing mitosis reach the restriction point/late G1 stage, as determined by pRb immunoreactivity. We used the cell-permeant dye FlashTag (FT) to label a cohort of pairs of sister cells that perform their division synchronously at E2, and counted the proportion of pRb-positive cells in the cohort in transverse sections from embryos harvested at different time points after FT injection. This proportion should reach a plateau when all the progenitors in the cohort have passed the restriction point and have become positive for pRb. At E2, this plateau was reached between 1.5 hours and 2 hours after injection, and the distribution of pRb immunoreactivity in FT-positive cells was stable at later time points (2.5 hours and 3 hours). This indicates that from 2 hours after mitosis injection, pRb-positivity is a reliable marker of progenitor status, and that a pair of cells containing 0, 1, or 2 pRb-positive cells correspond to a NN, PN and PP pair, respectively. For these experiments, a 1mM stock solution of FlashTag was prepared by adding 20µl of DMSO to a CellTrace Far red dye stock vial (Life Technologies, #C34564) as previously described (Baek et al., 2018). A working solution of 100µM was subsequently prepared by diluting 1µl of stock solution in 9µl of 37°C pre-heated PBS, and injected directly into E2 chick neural tubes. The eggs were resealed with parafilm and embryos were incubated at 38 °C for the appropriate time until dissection.

**3D reconstruction and measurement of cellular and mitochondrial volumes.**

Images of pairs of daughter cells at the first time point after division were imported as stacks in IMARIS software (Bitplane) to perform 3D reconstructions of cell volume and mitochondrial volume. Each daughter cell was individually segmented and reconstructed. Cells were delineated by drawing their contour on each z plane through their entire height using either the membrane reporter signal or a cytoplasmic reporter signal. With the contouring of the daughter cells, the cellular volume of each daughter cell was reconstructed using the surface creation tool of IMARIS. The mitochondrial signal contained in the cellular volume of each daughter cell was then isolated by masking mitochondrial signal located outside of this volume. Each daughter's mitochondrial volume was then reconstructed with the surface creation tool, using the same threshold for both cells. Data of both mitochondrial and cellular volumes for each daughter cells were then exported from Imaris to perform ratio measurements to assess the mitochondrial distribution between daughter cells and to compare their cellular volume.

**Forced attachment of mitochondria to kinesin using CatchFire**

We developed a time-controlled strategy to reversibly force mitochondrial attachment to the microtubular network (Figure 3A). The rationale was to restrict the perturbation to a time window around progenitor division in order to avoid long lasting effects on mitochondrial motility that may perturb their activity and be deleterious for daughter cell survival. The recently developed CATCHFIRE (chemically assisted tethering of chimera by fluorogenic-induced recognition) method is based on the reversible ligand-dependent dimerization of small genetically encoded protein partners. The smaller moiety of the dimer (FireTag) was fused to the N-terminus of the motor domain of the plus-end kinesin-like KIF17 (Bottone et al., 2023) (thereafter called KifFireTag). The larger moiety (FireMate) was anchored to mitochondria via the targeting sequence of the outer membrane protein Tom 20 (MitoFireMate, Figure 3A). The two partners can therefore enable the rapid and reversible association of mitochondria with the microtubule motor upon ligand administration and removal, respectively.

Embryos were electroporated at E1.5 with the appropriate plasmid combination (see above) and processed 24 hours later for en-face live-imaging according to the procedure described above. To induce the pairing of KifFireTag and MitoFireMate, a 20µM solution of ligand HMBR was prepared by diluting the original 20 mM stocks in F12 medium, and an appropriate volume was added to the culture dish to reach the desired final concentration of ligand. We first established a protocol of transient exposure of the sample to ligand-containing medium, that considers the diffusion kinetics of the ligand within the complex neuroepithelial tissue. Based on our previous experience with the HMBR ligand and pFAST, the fluorogenic monomeric parent of the CatchFire system, we expected that the diffusion of the ligand within the tissue would take between 15 and 30 minutes, and that it would display a slow disappearance kinetics after being washed out from the culture dish (Benaissa et al., 2021). We therefore anticipated that the induction and cessation of pairing of the CatchFire partners would follow a similar kinetics. We found that continuous exposure (1 hour) and/or high ligand concentration (10µM) led to aberrant mitochondrial distribution (Supplementary Figure 6B) and mitosis failure in several dividing cells. After several tests, we determined an optimal HMBR concentration (1µM) and duration of exposure (15minutes) after which ligand removal from the culture medium initiates a period of progressive depletion of the ligand from neuroepithelial cells. With this protocol, the intracellular ligand concentration appears to remain in the range of efficient CatchFire pairing for approximately 1 hour before the effect disappears (as judged from measurements of mitochondrial inheritance and compaction index (see Figure 3B and Supplementary Figure 6E.

In the final protocol used for fate tracking experiments, we started by selecting several fields of interest for imaging in the absence of the ligand. We then added ligand to the dish to reach a 1µM concentration in the medium. After 15 minutes, the ligand was removed from the culture dish by three gentle washes with 2 mL of HMBR-free F12 medium. We immediately started imaging progenitor divisions in the selected fields for 1 hour using the acquisition parameters described above in the "Live monitoring of mitochondria during cell divisions" section. After the 1-hour movie, we switched to the relevant acquisition parameters describe above in the "Daughter fate tracking experiments" section.

**Compaction index measurement**

The Compaction index (Ci) was determined using ImageJ software. Ci quantifies the effect of CatchFire pairing on mitochondrial compaction in dividing progenitors by measuring the ratio of a z-projection of the whole mitochondrial volume to the surface of the maximum cell contour at the time cytokinesis (Supplementary Figure 6D). The contour of the pair of sister cells was manually outlined from a 3µm z projection of the equator region where the daughter cell pair's surface area is maximum. Then a z projection of the total mitochondrial fluorescence from the pair of cells was performed, and contours of this fluorescence were manually drawn. For each pair of daughter cells, the ratio of the area occupied by mitochondria to the total area of the daughter cell pairs was calculated (Supplementary Figure 6D). According to our measurements in control progenitors in the absence of ligand (Supplementary Figure 6E), ratios below 0.6 were considered as compacted mitochondria cells while ratios above 0.6 correspond to cells with normal mitochondrial distribution.

**Vibratome section**

For vibratome sections, chick embryos were collected at desired stages in ice-cold PBS. Extraembryonic membranes were quickly removed and embryos were fixed for 1 hour in ice-cold 4%PFA/PBS and rinsed 3 times for 5 minutes in PBS at room temperature (RT). The trunk region was then dissected and embedded in 4% agarose (4g of agarose in 100ml of water, boiled in a microwave and cooled at 50°C). 100 µm vibratome sections were obtained using a Microm HM 650 V Microtome (ThermoScientific) and collected in 6-well plates in ice-cold PBS.

**Immunostaining**

Vibratome sections were incubated for one day with the primary antibodies diluted in PBS/0.1%triton (PBST) at 4°C with gentle agitation. Sections were then washed 3 times for 5 minutes in PBST at room temperature (RT), incubated overnight in the dark at 4°C with the

appropriate secondary antibodies (and DAPI if needed) diluted in PBST, washed again 3 times for 5 minutes at RT with PBST and mounted with Vectashield (Vector Laboratories H-1000-10). Primary antibodies used are: rabbit anti-pRb (Ser807/811 – 1:1000) from Cell Signaling; mouse anti-HuC/D (clone 16A11 – 1:50) from ThermoFisher Scientific; Chick anti-GFP (1/800) from Aves Labs. Secondary antibodies coupled to Alexa Fluor 488 (1:500), Alexa Fluor 566 (1:500) or Alexa Fluor 649 (1:250) were obtained from Jackson laboratories.

Mitochondrial distribution upon ligand administration during progenitor division.

En-face culture of the embryonic neuroepithelium was performed as described in the "En-face culture" section above with one additional step during the experimental procedure: dissected neural tubes were incubated in a SiR-tubulin solution (SC006: Cytoskeleton Kit, tebu-bio; 1µM final concentration in F12 culture medium) during 1 hour at 37°C before flat-mounting. The culture dish was transferred to the 38 °C chamber of a spinning disk confocal microscope and filmed as described above in the "Live monitoring of mitochondria during cell divisions" section. Divisions were imaged before ligand administration for the control condition, and after removal of the ligand (HMBR 5µM) for the CatchFire condition.

**Key Ressources Table – STAR METHODS**

| REAGENT OR RESSOURCE | SOURCE | IDENTIFIER |
|---|---|---|
| Antibodies | | |
| Chick anti-GFP | Aves Labs | Cat#GFP-1020 RRID : AB_10000240 |
| Rabbit anti-pRb (Ser807/811) | Cell Signaling | Cat# 8516S RRID : AB_331472 |
| Mouse anti-HuC/D (clone 16A11) | ThermoFisher Scientific | Cat#A-21271 RRID : AB_221448 |
| **Softwares** | | |
| ImageJ | (Schneider et al., 2012) | http://imagej.net/Welcome RRID: SCR_003070 |
| Graphpad Prism | Graphpad | http://www.graphpad.com/ RRID: SCR_002798 |
| Microsoft Excel | Microsoft | RRID: SCR_016137 |
| MicroManager | (Edelstein et al., 2010b) | https://micro-manager.org/ RRID: SCR_000415 |
| Affinity Publisher | Affinity | N/A |

## Table S1: List of plasmids used in this study

| Plasmids | # | Remarks | ref |
|---|---|---|---|
| pCX-mbGFP-ires-H2BGFP | X411 | (Membrane + Histone H2B) GFP | This study |
| pCX-mbiRFP670 | X71 | Membrane iRFP670 | This study |
| pCX-ZO1-miRFP670 | X786 | ZO1 iRFP670 | This study |
| pCX-H2B-EGF | X014 | Histone H2B GFP | Hadjantonakis et al 2004 |
| PMP-cdc25b | X521 | Human CDC25B3 under control of the pccRE element of the mouse cdc25b promoter | Bonnet et al 2018 |
| PMP-lacZ | X1090 | Control vector expressing lacZ under control of the pccRE element of the mouse cdc25b promoter | Bonnet et al 2018 |
| cdkn1c SH1 | X1101 | Chick CDKN1c miRNA under control of chick U6 promoter, H2B-EGFP under control of CAGGS promoter | Mida et al |
| shCTRL | KD048 | Control miRNA targeting the luciferase sequence under control of chick U6 promoter, H2B-EGFP under control of CAGGS promoter | Peyre et al, 2011 |
| Cytobow (EF) | X400 | | Loulier et al 2014 |
| MitoBow (EF) | X503 | | Loulier et al 2014 |
| pCX-Mito-CFP | X508 | Expresses a mECFP-tagged mitochondrial reporter (Cox8-mECFP) | Unpublished, gift from Jean Livet |
| pCX-lox-H2B-EBFP-lox-mitoEGFP | X1017 | Cre-recombinase dependent expression of GFP-tagged mitochondrial reporter (Cox8-mEGFP). | This study |
| pCX-lox-mitoCherry-lox-mitoEGFP | X1018 | Constitutive expression of a mCherry tagged mitochondrial reporter (Cox8-mCherry1), and Cre-recombinase dependent expression of GFP-tagged mitochondrial reporter (Cox8-mEGFP). | This study |
| pCX-Mito-Cherry | X1202 | mCherry-tagged mitochondrial reporter (Cox8-mCherry1) | This study |
| pCX-Cre | X022 | Constitutive expression of the Cre recombinase under control of the CAGGS promoter | Morin et al, 2007 |
| pCX-Tom20-NpFAST | X1273 | TOM20-NpFAST (MitoFireMate) | This study |
| pCX-Kif17a-CpFAST | X1274 | Kif17a-CpFAST (KifFireTag) | This study |
| cTis21-p2A-NLSCre | X907 | donor vector for somatic knock-in of Cre recombinase in the chick Tis21 locus | Petit-Vargas et al |
| pCX-SpCas9-cTis21-gRNA2 | X854 | Expresses a gRNA targeting the C-terminus of the chick Tis21 locus under control of human U6 promoter, and the SpCas9 nuclease under control of the hybrid CMV-Chicken b-actin promoter | Petit-Vargas et al |

## Figure legends

### Figure 1: Increased frequency of uneven mitochondrial inheritance at the onset of asymmetric modes of divisions during neurogenesis

**A.** Scheme of in ovo electroporation of DNA constructs in the chick embryonic neural tube and experimental strategy for open-book live imaging in the electroporated neural tube.

**B.** En-face time lapse monitoring of mitochondria (red) and cell contours (cyan) in a dividing neural progenitor. Scale bars 5µm.

**C.** En-face confocal images and 3D reconstructions of mitochondrial volume in sister cells immediately after cytokinesis. 3D reconstructed images from the entire z-stacks are used to calculate the ratio $R_{mito}$ of mitochondrial inheritance between sister cells. Typical examples of even (i) and uneven (ii) inheritance are depicted. Scale bars 5µm.

**D.** Left: scatter plots of $R_{mito}$ distribution at E2, E3 and in Tis21 positive progenitors (E3, Tis21-Cre). Light color bars represent the percentage of cell pairs in each 0.5 interval. Statistical analysis: Kruskal-Wallis ***: p=0.0003(distributions between E2, E3 and E3, Tis21-Cre), Mann-Whitney. ***: p=0.001. *: p=0.026 (E2-E3) and *: p=0.015 (E3 and E3, Tis21-Cre). Right: schematic representation of the CRISPR/Cas9 knock-in strategy of the Cre recombinase used to activate a loxP-dependent mitochondrial reporter specifically in Tis21 neurogenic progenitors.

## Bunel et al., Figure 1

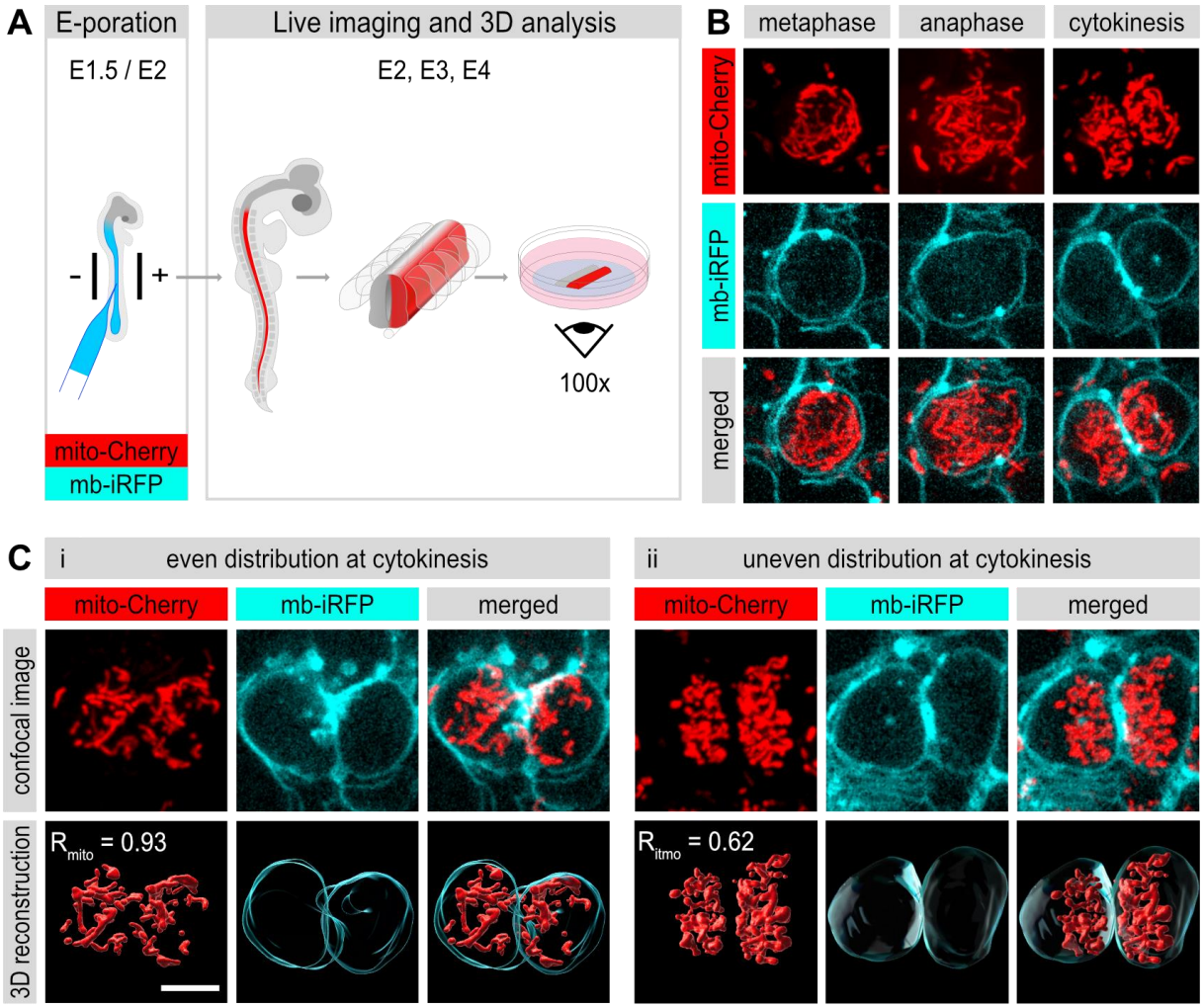


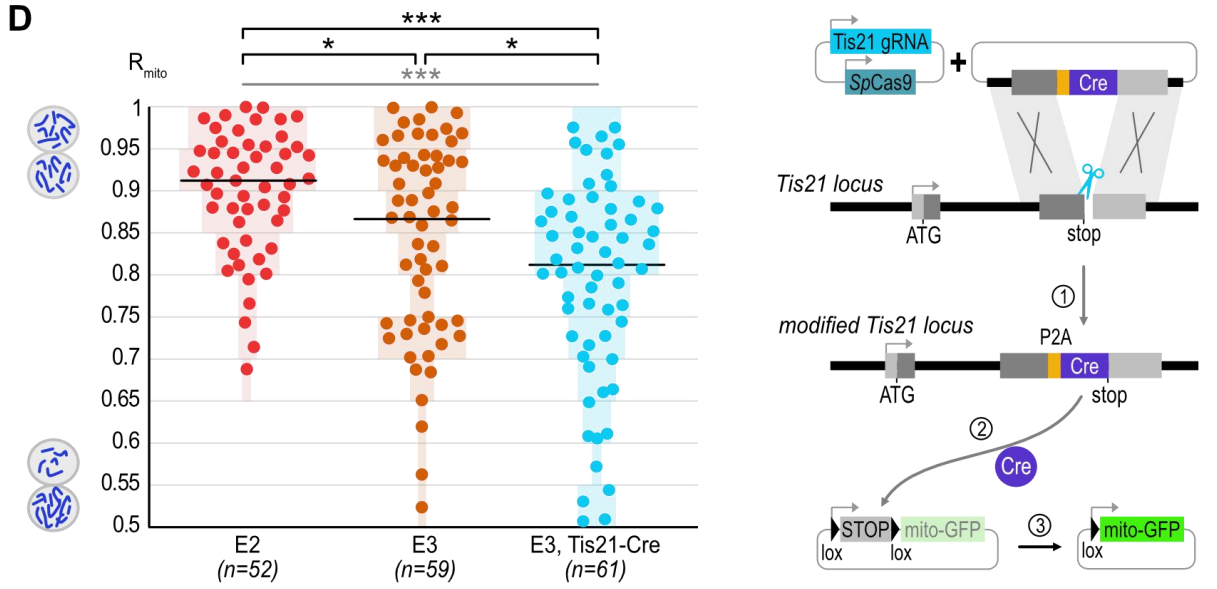

**Figure 2: Unequal mitochondrial inheritance by sister cells is a hallmark of asymmetric division**

**A.** Scatter plots of $R_{mito}$ in sister pairs of control cells and upon overexpression of CDC25b at E2.5. Mann-Whitney. *: p=0.004.

**B.** Scatter plots of $R_{mito}$ in control cells and upon downregulation of CDKN1c at E3. Control cell values at E3 are identical to Figure 1D. Mann-Whitney. *: p=0.019. Light color bars in A and B represent the percentage of pairs in each 0.5 interval.

**C.** Experimental strategy combining live monitoring of mitochondrial inheritance and daughters fate tracking.

**D.** Time-lapse series linking mitochondrial distribution and mode of division in Tis21 positive progenitors. Scheme (top) and en-face view (middle) of the time course from progenitor division to daughters' fate determination (division: progenitor, delamination: neuron). Bottom: uneven mitochondrial inheritance ($R_{mito}$=0.61) matches with an asymmetric PN fate in sister cells: Scale bar: 5µm.

**E.** Scatter plots summarizing $R_{mito}$ and daughter fate (P=progenitor, N=neuron) from Tis21-positive progenitors. Red line: ($R_{mito}$ = 0.85) proposed threshold separating equal from unequal inheritance.

**F.** Inheritance of the smallest mitochondrial pool by the future neuron (full dots in E) or progenitor (open circles in E) in 23 PN pairs with unequal mitochondrial segregation.

**Bunel et al., Figure 2**

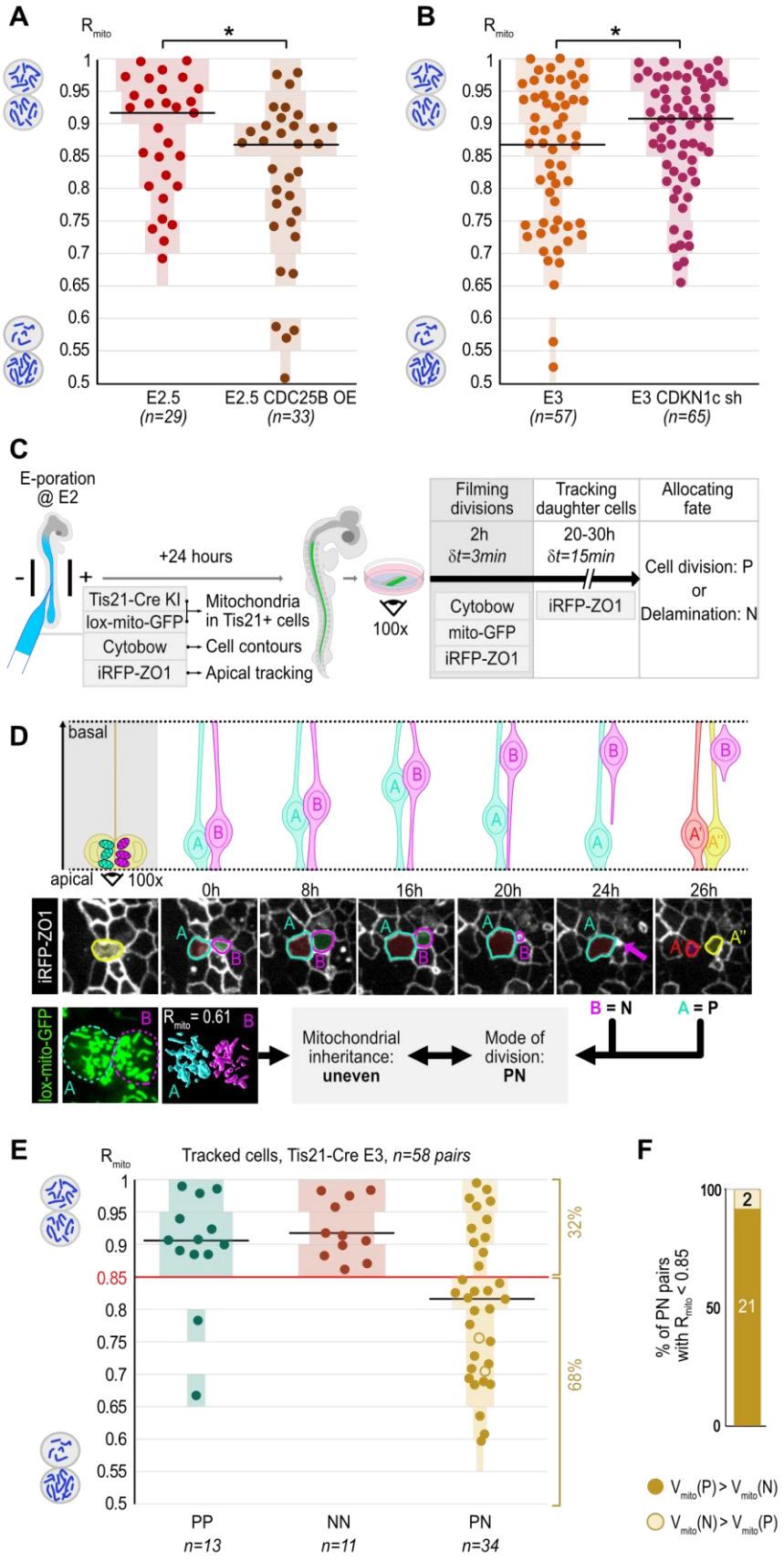

**Figure 3: Forced unequal mitochondrial inheritance induces asymmetric fate choices**

**A.** Scheme of the CatchFire strategy to force mitochondrial attachment to the microtubular network during mitosis.

**B.** Scatter plots of $R_{mito}$ in CatchFire condition before, with (double arrow) and after washout of ligand. Green box: estimated period of ligand activity in cells. N=80 pairs.

**C.** Combined live monitoring of mitochondrial inheritance and daughter cell fate tracking at E2.5.

**D.** Scheme (top) and en-face views (middle) of daughter cell's nucleus (H2B-GFP, white) in the depth of the neuroepithelium during the live tracking period (left) and correspondence with pRb immunofluorescence at its end (right, magenta). Bottom: $R_{mito}$=0.78 in the mother cell matches with PN fate: Scale bar: 5µm.

**E-G.** Representations of $R_{mito}$ and/or cell fate data from control (n=40 pairs) and CatchFire cells (n=36 pairs) obtained from the two tracking approaches. Percentages of $R_{mito} < 0.85$ vs $> 0.85$ (E) and fate (F). Numbers in columns represent the number of pairs. G: Scatter plots summarizing $R_{mito}$ and daughter fate data. Squares in the CatchFire condition indicate a mitochondrial compaction index (Ci)< 0.6. Open symbols in PN pairs: smallest pool inherited by progenitor. P=progenitor, N=neuron. Chi2 test: E, p=0.0005 ; F, p=0.006.

**Bunel et al., Figure 3**

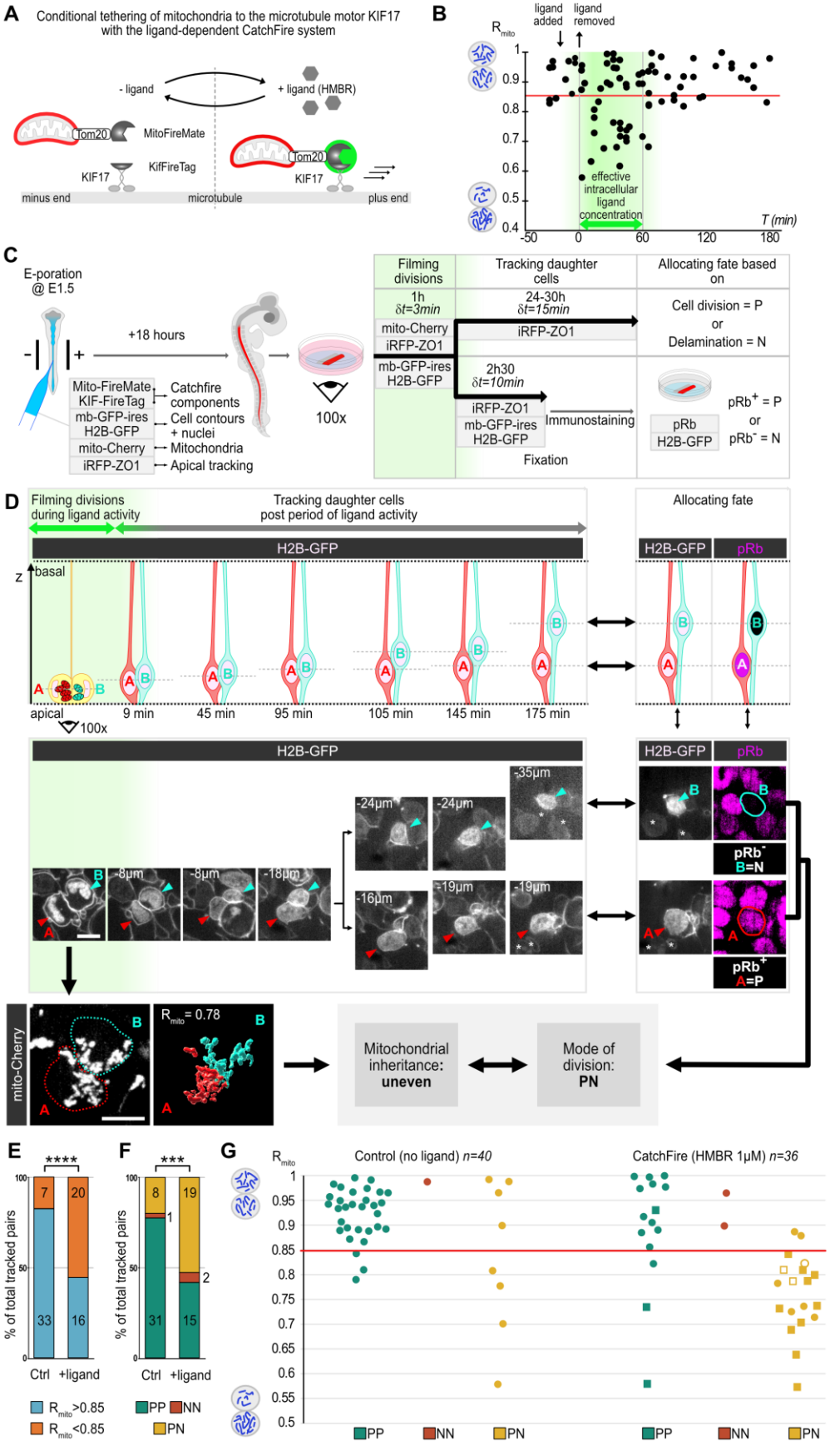

**Legends to Supplementary Figures**

**Supplementary Figure 1: 3D reconstruction of mitochondrial volume in daughter cells from a neural progenitor.**

A. En-face view of a 90*90µm of a single field of a neural tube in live imaging at two different time points. Red : Mitochondria , Cyan:cell contour.

Representative images and 3D reconstructions of mitochondria distributed evenly (i, $R_{mito}$ = 0.97) in (white box in the upper panel) or unevenly (ii, $R_{mito}$ = 0.71) in the daughter cells of the progenitor highlighted in the dashed white box on the upper left panel and in full line in the upper right panel between daughter cells of dividing progenitors at E2. Upper rows: z plane of cell contour and chromosomes (middle, cyan), mitochondria (left, red), and merged (right) live fluorescence; Bottom row: corresponding 3D reconstructed images from the entire z-stacks. Scale bars 5µm.

**B. 3D reconstruction pipeline:** Stack file of images of daughter cells immediately after division (~25µm deep z-stacks with a 0.3µm z-step) were imported in IMARIS software (Bitplane) to perform cell volume and mitochondrial volume 3D reconstructions. Each daughter cell volume was delineated manually by drawing cell contour on each z plane through their entire height using either the membrane reporter signal or a cytoplasmic reporter signal, and reconstructed using the surface creation tool of IMARIS. The mitochondrial signal contained in the cellular volume of each daughter cell was then isolated by masking mitochondrial signal located outside of this volume. Each daughter's mitochondrial volume was then reconstructed with the surface creation tool, using the same threshold for both cells. Data of mitochondrial volumes for each daughter cells were then exported from Imaris to perform ratio measurements to assess the mitochondrial distribution between daughter cells.

**Bunel et al., Supplementary Figure 1**

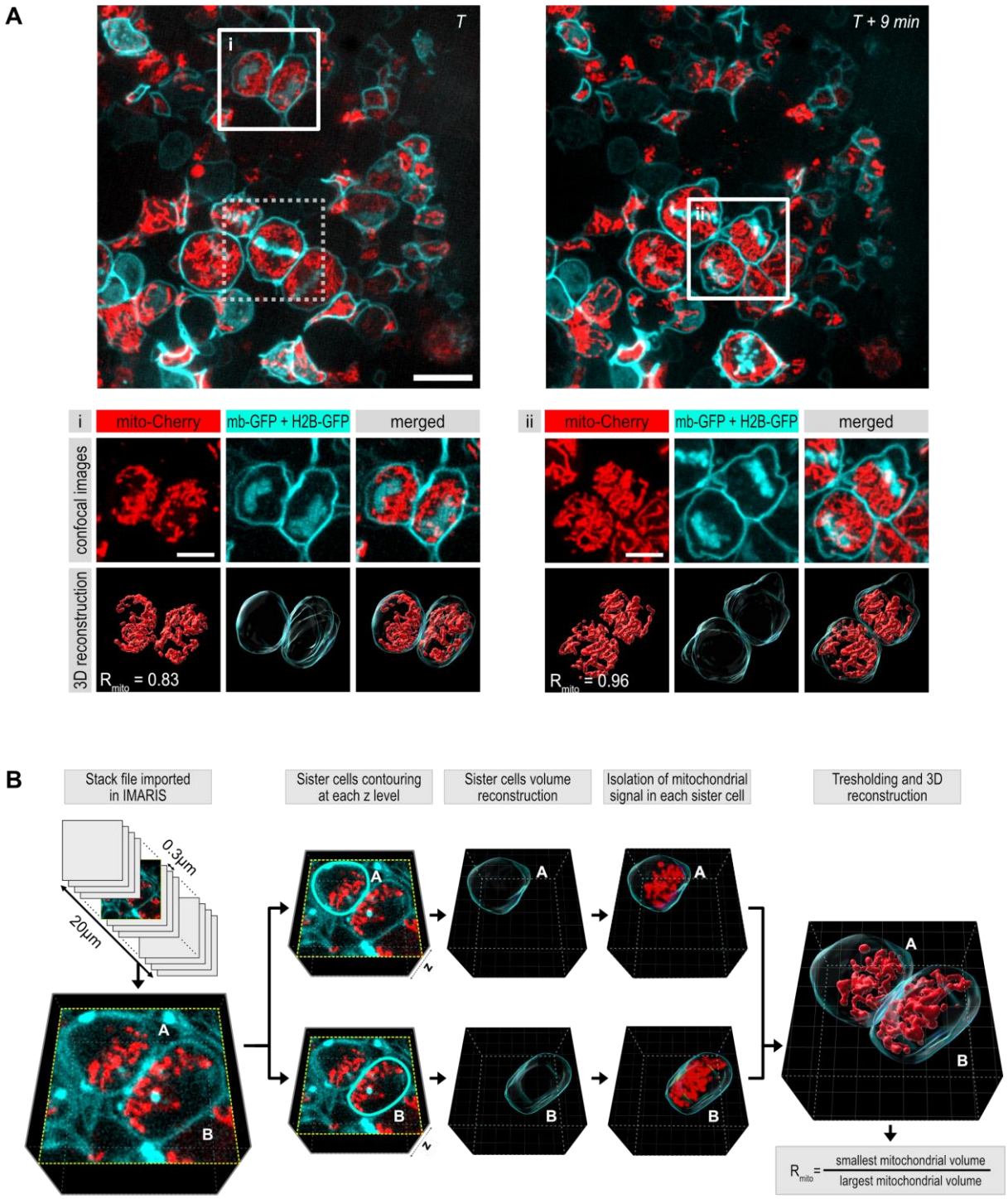


**Supplementary Figure 2: Absence of correspondence between mitochondrial inheritance ratios and cell volume ratio.**

**Left:** 3D reconstruction of cell volume in pairs of daughter cells born from a neural progenitor. Stack file of images of daughter cells immediately after division (~25µm deep z-stacks with a 0.3µm z-step) were imported in IMARIS software (Bitplane) to perform cell volume and mitochondrial volume 3D reconstructions. Each daughter cell volume was delineated manually by drawing cell contour on each z plane through their entire height using either the membrane reporter signal and reconstructed using the surface creation tool of IMARIS. The mitochondrial signal contained in the cellular volume of each daughter cell was then isolated by masking mitochondrial signal located outside of this volume. Each daughter's mitochondrial volume was then reconstructed with the surface creation tool, using the same threshold for both cells. Data of both mitochondrial and cellular volumes for each daughter cells were then exported from Imaris to perform ratio measurements to assess the mitochondrial distribution between daughter cells and to compare their cellular volume.

**Right:** Ratios of mitochondria volumes ($R_{mito}$) are plotted on the left line. The corresponding cell volume ratios ($R_{cell}$) are plotted on the right line. Magenta marks pairs in which the cell inheriting the smallest mitochondrial volume (B) is smallest than its sibling (A). Green marks pairs in which the cell inheriting the smallest mitochondrial volume (B) is larger than its sibling; in this case, $R_{cell}$ corresponds to the ratio between the volume of cell A over the volume of cell B. N=60**.**

**Bunel et al., Supplementary Figure 2**

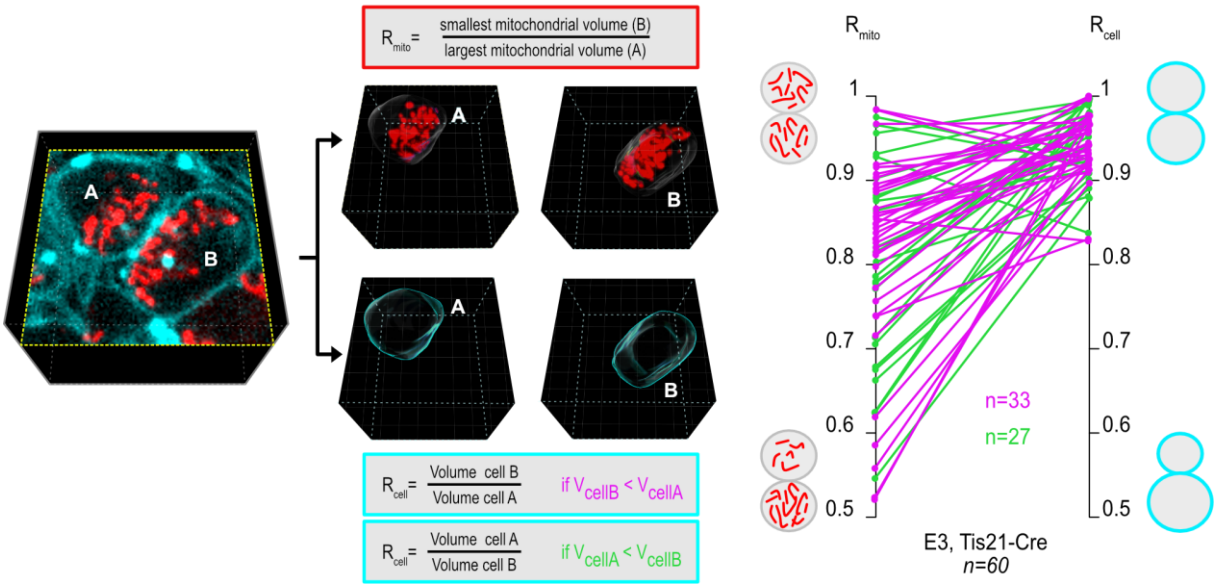

**Supplementary Figure 3: Increased neurogenesis upon Cdc25b overexpression in the chick embryonic neural tube.**

**Left:** Distribution of the pRb positive cells (light blue), pRb/HuC-D double negative cells (green) and HuC-D positive neurons (dark blue) in control or CDC25b overexpression (CDC25b OE) conditions at E3, 30 hours after electroporation (30 hours post EP). N=4 embryos for control and N=3 embryos for CDC25b OE conditions. Statistical analysis was performed using Mann-Whitney test *****: $p < 0.0001$.

**Right:** Transverse sections of the electroporated chick neural tube (thoracic level) at E3 Immunofluorescence with HuC-D antibody to label neurons (magenta, cytoplasmic signal) and pRb to label progenitors (magenta, nuclear signal) (right panels) in control and overexpression of CDC25b conditions. H2B-GFP fluorescence (middle panels, green) represents the fluorescent electroporation reporter and DAPI staining is showed in blue (left panels). Scale bars: 50µm

## Bunel et al., Supplementary Figure 3

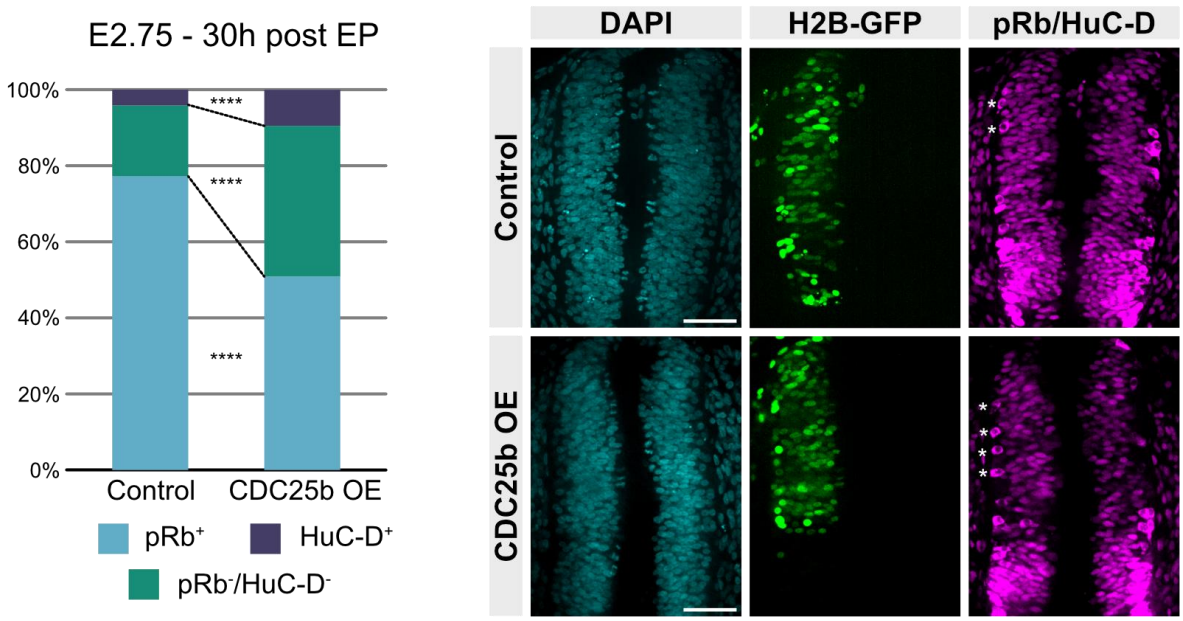

**Supplementary Figure 4: Fate tracking in pairs of daughter cells from a Tis21 positive progenitor showing even mitochondrial distribution and symmetric modes of division**

**A. Experimental strategy to combine live monitoring of mitotic mitochondrial inheritance and tracking of daughter cell fate.** *In ovo* electroporation of a combination of five vectors carrying DNA constructs for Tis21-P2A-Cre somatic knock-in, and fluorescent reporters for mitochondria (lox-mito-GFP), apical tracking (iRFP-ZO1) and cytoplasm staining (Cytobow) in the chick embryonic neural tube at E2. Embryos were harvested at E3, and neural tubes were flat-mounted for en face view imaging. The neuroepithelium was imaged at high spatio-temporal resolution (δt=3min and z=0.3µm) for two hours to record mitochondrial inheritance during progenitor divisions, followed by tracking of the daughter cells by imaging the apical surface at lower resolution (δt=15min and z=1µm, 20µm stack height centered on iRFP-ZO1 staining) for 20 to 30 hours.

**B-C**. **Time-lapse series (en-face imaging) of dividing neural progenitors showing even mitochondrial distribution and symmetric modes of division (B and C)**

Top rows: Schematic representation of the time course from the division of a progenitor to the determination of its daughter's fate based on their behavior and morphological criteria (new division for a progenitor, delamination for a neuron). Middle rows show time-lapse series (en-face imaging) of the iRFP-ZO1 signal used for long term tracking of pairs of daughter cells. In panel B, both daughter cells A and B are progenitors (as deduced from their division producing A' and A'', and B' and B''), while in panel C, both daughters are neurons (as deduced from the progressive reduction of their apical surface followed by delamination at 24h and 28h). Bottom rows: mitochondrial distribution is measured during division of the mother cell and matched with the mode of division deduced from the fate of the daughters. Scale bars in B-D: 5µm.

# Bunel et al., Supplementary Figure 4

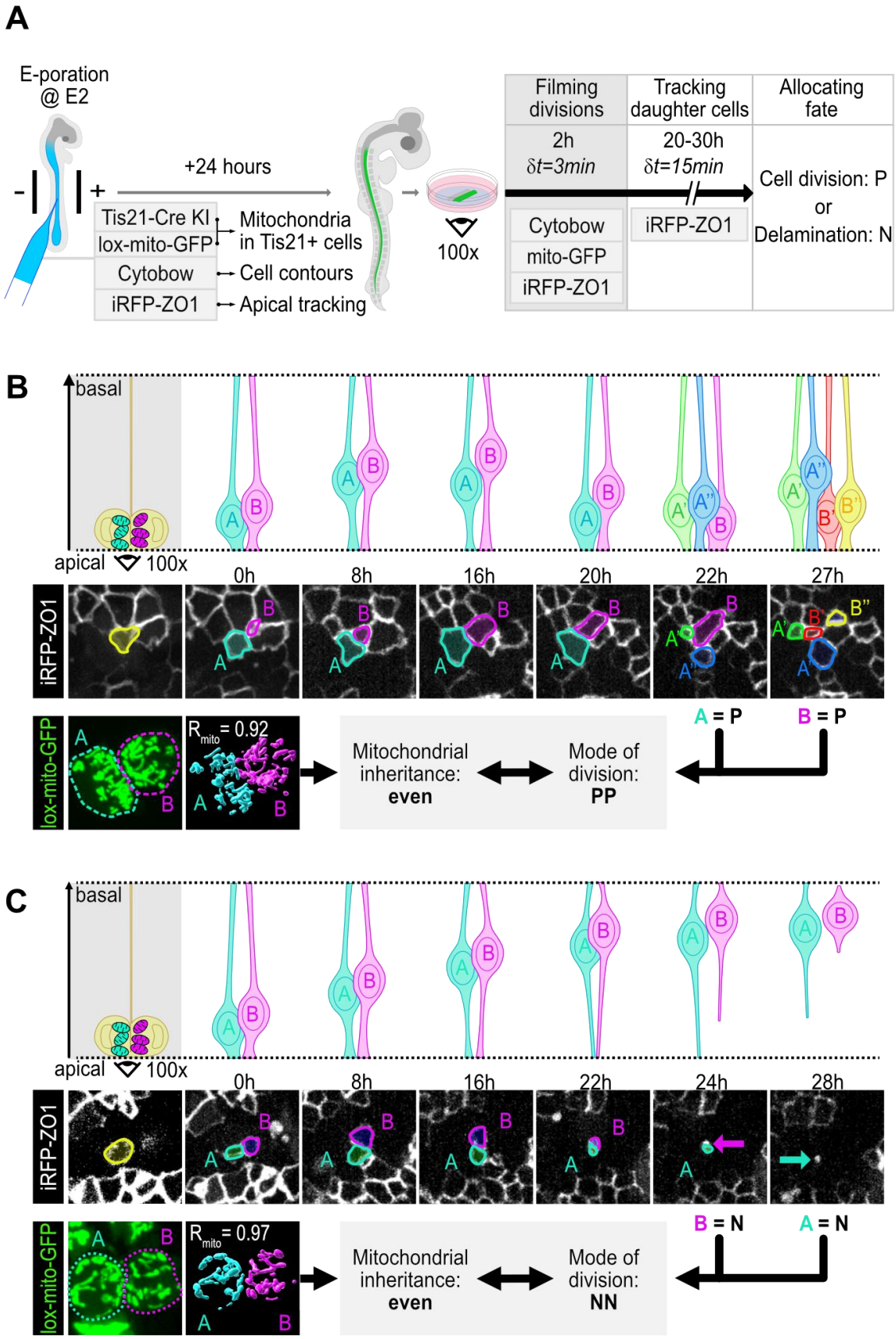

**Supplementary Figure 5: Mitochondrial behavior and localization during metaphase and anaphase are modified in CatchFire electroporated cells upon ligand (HMBR) administration.**

z-projections (2.5µm corresponding to 5 z-levels) at three different levels (top, middle and bottom) of dividing progenitors, (see schematic representation in the middle panels) during metaphase, (upper panels) and anaphase (lower panels). Mitochondria (mito-Cherry, red), which are typically dispersed throughout the cytoplasm of the mitotic cell in metaphase in control conditions (left panels), are concentrated more basally in ligand exposure conditions (right panels). In anaphase, mitochondria appeared more compacted at the cleavage furrow upon ligand administration (right panels) compared to the control situation (left panels). Scale bars: 5µm

**Bunel et al., Supplementary Figure 5**

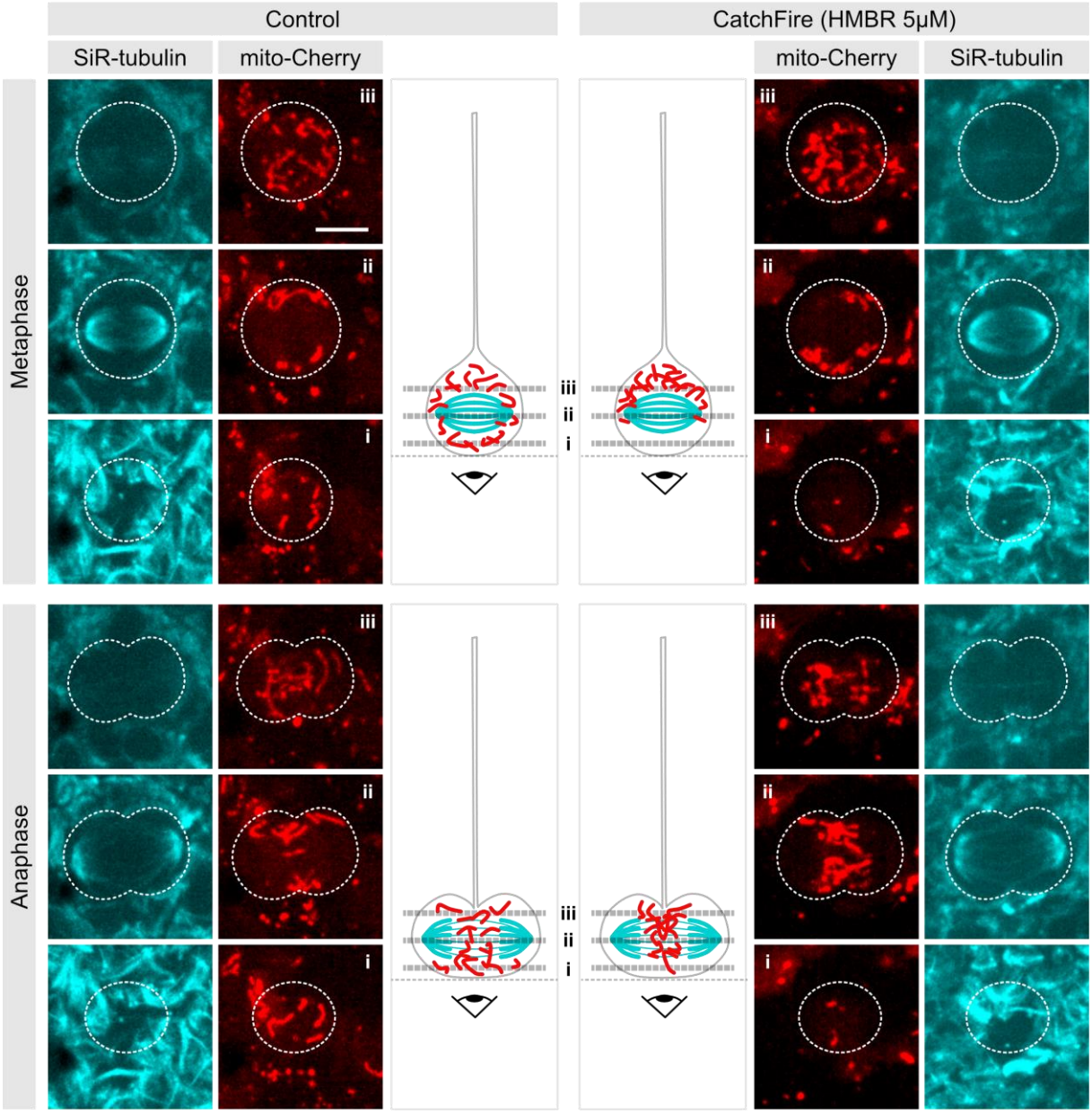


**Supplementary Figure 6: CatchFire-induced mitochondria/Kif17 interactions modify mitochondrial behavior and localization**

**A. Visualization of the sites of mitochondria/kif17 interaction in telophase.** The interaction between the two partners (Tom20-FireMate, Kif17-FireTag) in the presence of the HMBR ligand is visualized via green fluorescence (HMBR, green) (see Figure 4), which colocalizes with an independent mitochondrial reporter (Cox8-Cherry, yellow). The signal also partially colocalizes with the microtubular network (SiR-tubulin, cyan). Mitochondria are more compacted at the cleavage furrow in ligand exposure conditions (middle and lower panels) compare to control condition (upper panels). Scale bars: 5µm.

**B. Graphical representation of mitochondrial ratios over time during continuous exposure to the HMBR ligand at high concentration (10µM).** Each dot represents a mitochondrial ratio. The red line shows the threshold between "equal" and "unequal" $R_{mito}$ values (0.85) and the blue line shows the lower limit of $R_{mito}$ observed in control conditions. Open circles show cases of $R_{mito}$ lower than 0.5, indicating an extreme imbalance in mitochondrial inheritance that is never observed in control conditions. The ligand was added to the culture medium at T=0min and maintained in the culture during the entire experimental period.

**C. Scatter plots of $R_{mito}$ in CatchFire condition before and after (Control) and during the estimated 1hour period of effective intracellular CatchFire ligand concentration** defined in Figure 3B. Gray and green color bars represent the percentage of cell pairs in each 0.5 interval. Data are the same as in Figure 3B. Statistical analysis: Mann-Whitney. *: p=0.0137 n=80 pairs.

**D. Schematic representation of the measurement of the Compaction index (Ci),** illustrated by live imaging of dividing progenitors (upper panels). To determine Ci, we used a z-projection of the total mitochondrial signal from the whole cellular volume (mito-cherry, red) and a z-projection of the maximum cell contour (3 to 5 z-levels at the cell's equator; mb-GFP, green) at the time cytokinesis. The contours of the projected cell and mitochondrial surfaces were manually drawn (middle panel, green and red respectively). Ci is calculated as the ratio of the corresponding surfaces (mitochondrial over equatorial cell surface of the daughter cell pairs). Examples of control (top) and HMBR treated (bottom) sister cells are shown. Scale bars: 5µm.

**E. Graphical representation of Ci in cells electroporated with the CatchFire components**, measured before (-50 to -15 min) and after (-15 to 0 min) addition of the ligand to the medium and following ligand washout from the medium (0 to 200 min). Each dot represents Ci for 1 pair of sister cells. Many cases of Ci values lower than 0.6 (green dots) are observed during a 1hour time window after ligand removal from the medium (green box), whereas all values are

higher than 0.6 before and after this time window. This corresponds to the time period during which we observed low values of $R_{mito}$ in the same experiment (also marked with a green box in Figure 3B). Blue dots represent pairs during ligand exposure with a Ci similar to the control condition. Bottom: Scheme of the theoretical variation of the intracellular ligand concentration during the experimental period. Data are from the same dataset as in panel C and in Figure 3B, except that Ci could not be measured in one control pair. N=79 pairs.

**F. Graphical representation of the relationship between $R_{mito}$ and Ci values measured at E2.5** in cells electroporated with the CatchFire components, corresponding to the experimental dataset depicted in panels C and E and in Figure 3B. Blue and green dots correspond to cells dividing during the 60' time window highlighted by the green box in panel E and Figure 3B. Note that in this population, all the green cells with a Ci value lower than 0.6 which is never observed in the control population display a $R_{mito}$ lower than 0.85, whereas most of the blue dots have similar $R_{mito}$ as the control population. N=79 pairs.

**Bunel et al., Supplementary Figure 6**

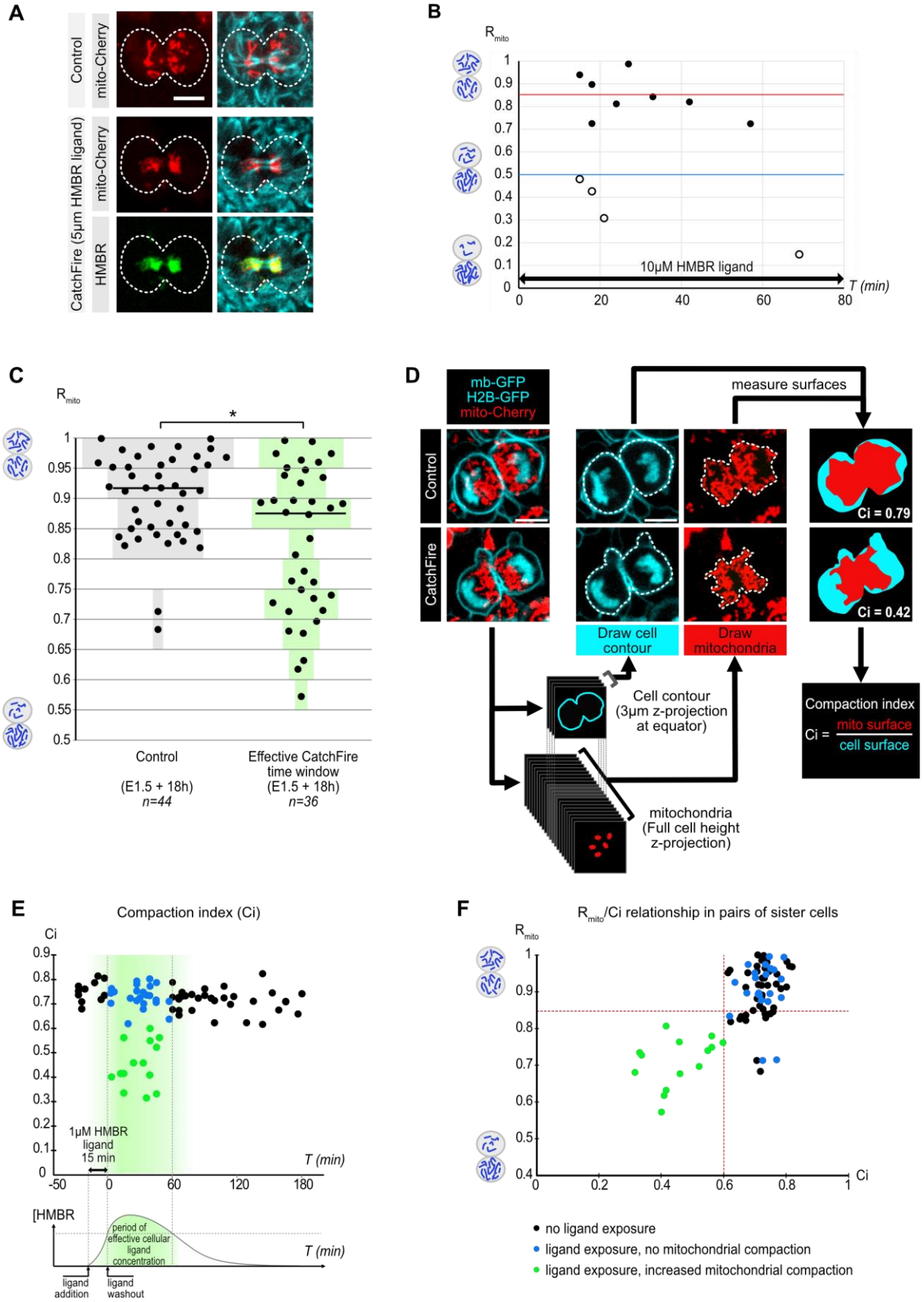

**Supplementary Figure 7: Forced unequal mitochondrial inheritance induces asymmetric fate choices**

Representative examples of a NN division **(A)** and a PP division **(B)** both displaying a characteristic even mitochondrial inheritance.

Scheme (top) and confocal en-face views (middle) of daughter cell's nucleus (H2B-GFP, white) in the depth of the neuroepithelium during the live tracking period (left) and correspondence with pRb immunofluorescence at its end (right, magenta).

Bottom: $R_{mito}$ value measured upon cytokinesis of the mother cell is matched with daughter cells fate deduced from tracking: Scale bar: 5µm.

**Bunel et al., Supplementary Figure 7**

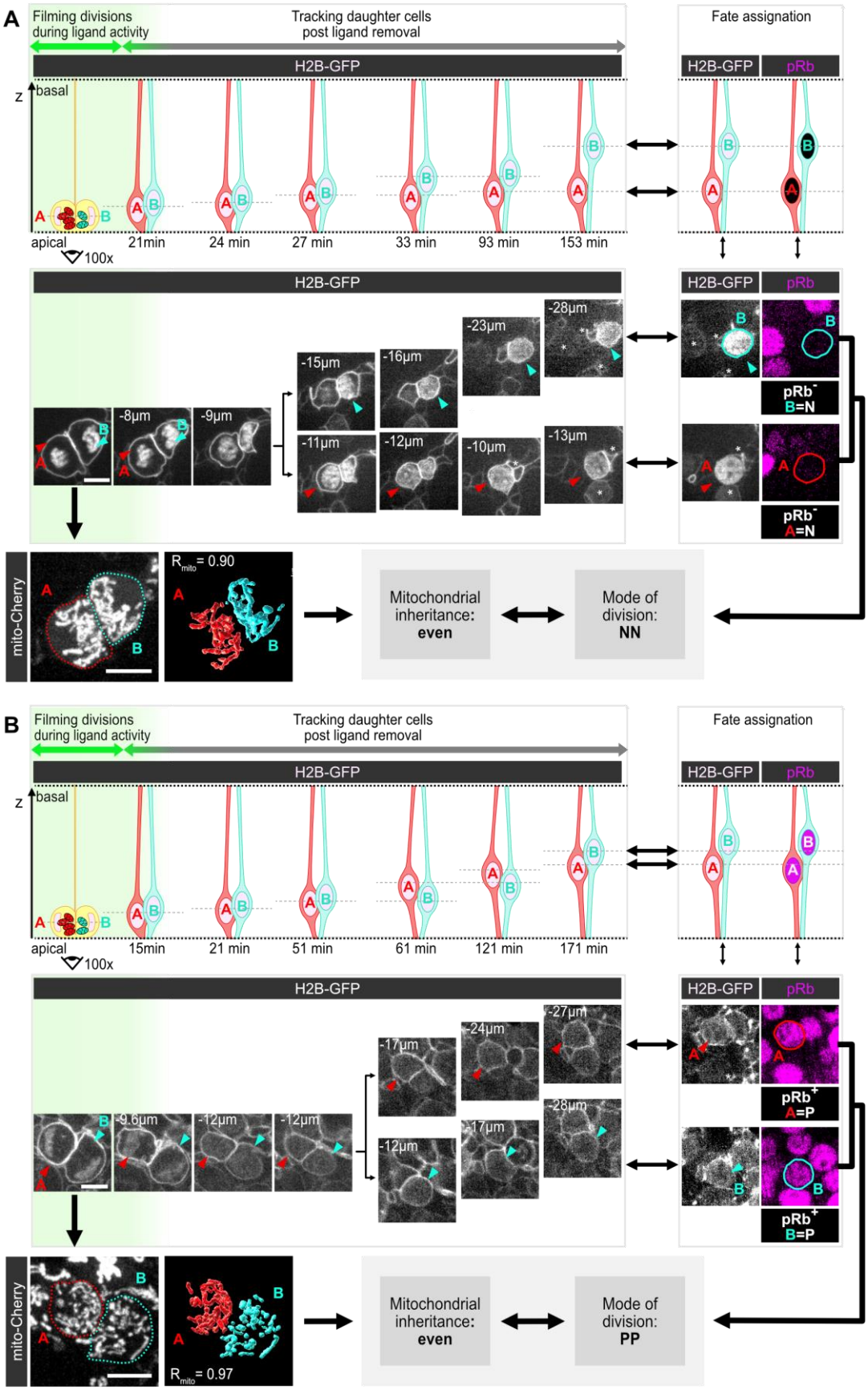

**Supplementary Figure 8: Forced unequal mitochondrial segregation in progenitors dividing mostly symmetrically leads to differential cell fate in daughter cells**

**A. Graphical representation of percentages of divisions displaying $R_{mito}$ values higher versus lower than 0.85 in the live tracking experiments** in control and CatchFire conditions, from the long-term live tracking (top) and from the combined short tracking and immunostaining (bottom) experiments. Numbers indicated in columns correspond to cell numbers. Data are from the same experiments presented in a combined format in Figure 3E.

**B. Graphical representation of percentages of PP, PN and NN pairs of sister cells** in control and CatchFire conditions in the live tracking experiments, from the long-term live tracking (top) and from the combined short tracking and immunostaining (bottom) experiments. Numbers indicated in columns correspond to cell numbers. Data are from the same experiments presented in a combined format in Figure 3F.

**C. Correspondence between mitochondrial inheritance and fate of daughter cells** in control and CatchFire conditions. The datasets obtained from the two independent methods for fate assignation based either on long term live tracking (n=19 control cells and n=19 cells in CatchFire condition) or on combined short tracking and immunostaining (n=21 control cells and n=17 cells in CatchFire condition) are presented in the upper and lower rows respectively. They are from the same experiments presented in a combined format in Figure 3G.
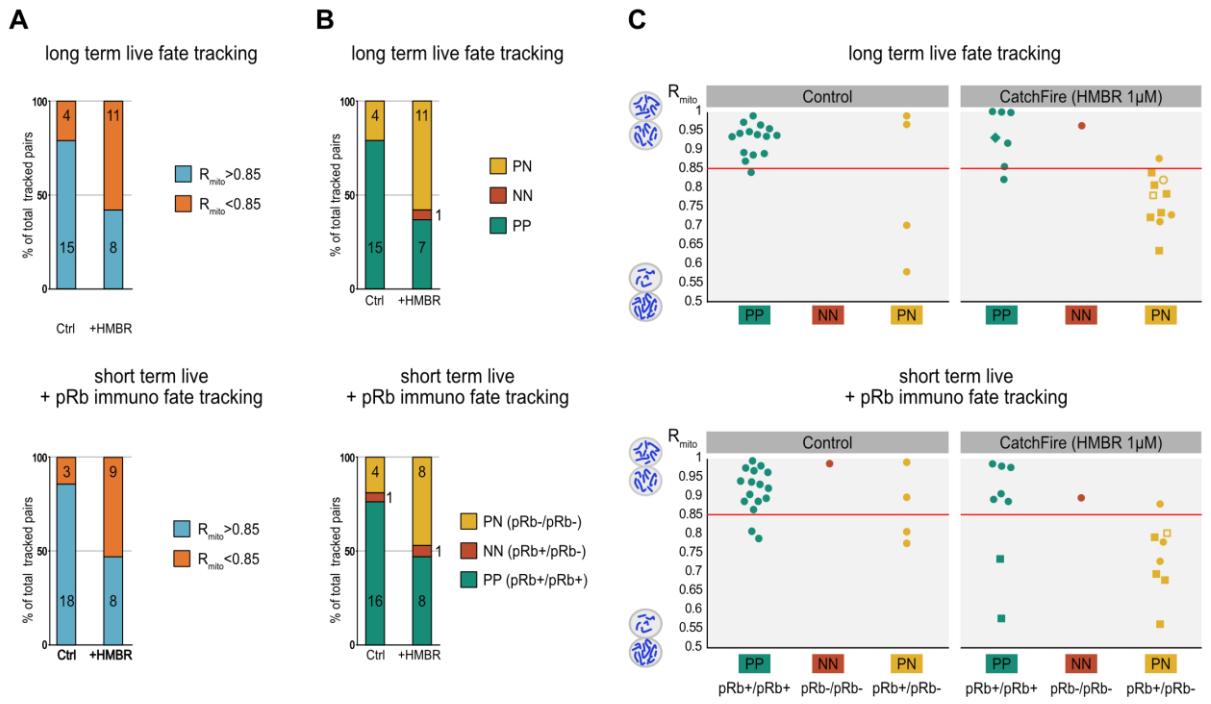
**Bunel et al., Supplementary Figure 8**